Springer Praxis Books

Light Scattering Reviews 5

Single Light Scattering and Radiative Transfer

Bearbeitet von
Alexander Kokhanovsky

schnell und portofrei erhältlich bei

2 Application of scattering theories to the characterization of precipitation processes

Sandra Jacquier and Frédéric Gruy

2.1 Introduction

Solid–liquid suspensions are frequently used in industrial processes. These suspensions usually contain aggregates made up of solid primary particles. Many characterization tools of these suspensions are based on light scattering (Mie theory). However, Mie theory (1908) is not always applicable to practical problems since the scatterer must be a homogeneous sphere. The ordinary particle sizers that use this theory do not make it possible to measure non-spherical particle geometrical characteristics. Extensions of the Mie theory for arbitrary shaped particles or particle aggregates are available nowadays (the T-matrix method, the Generalized Multiparticle Mie (GMM)-solution, etc.). But the computing times of the optical properties via these exact theories do not allow for a real-time analysis. This chapter is therefore dedicated to the search for approximate methods for the estimation of aggregate optical properties, particularly their scattering cross-section.

This chapter is split into five main sections. Section 2.2 concerns the aggregation process and, more generally, the precipitation process, to provide a better understanding of the framework of this study. Precipitation is the formation of a solid in a solution during a chemical reaction. The morphology of particles currently observed during precipitation or particle synthesis will be described. The relationship between optics and particle technology will be recalled. Section 2.3 outlines briefly the different approximate methods used for the case of spherical and non-spherical particles. Section 2.4 presents selected approximations for light scattering cross-sections in the case of aggregates. The quality of each approximation will be discussed by comparison with the exact theory. Practical cases will be presented. Section 2.5 is an extension of the previous section to the light pressure cross-section. Section 2.6 is an attempt to relate the scattering properties of aggregates to their geometrical characteristics.

In the next section we describe the context of the need for approximate methods for scattering cross-section of aggregates.

2.2 Aggregate formation

Materials are often made from inorganic particles. These are formed by reactions in the gas phase or, more commonly, in liquid phases. The main process is called precipitation.

2.2.1 Precipitation and particle synthesis

The classical situation is the following: a solution consisting of a solute A and a solvent is mixed with another one consisting of a solute B and the same solvent. The two solutes react to form a solid product denoted AB.

$$A + B \leftrightarrow AB.$$
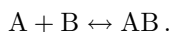
A and B are often ions.

If equilibrium between the solid phase and the solutes is reached, thermodynamics tells us that this equilibrium (saturated solution) is characterized by the solubility of the solid phase. However, when the concentrations of A and B are high enough to produce solid particles, the initial solution is supersaturated. So, the ratio of the actual concentration and the equilibrium concentration (solubility), called supersaturation, is the key parameter of the dynamics of precipitation. The higher the supersaturation, the higher the precipitation rate. Particle formation can be distinguished into three stages: nucleation, growth and agglomeration.

Nucleation is the birth of particles that are large enough to grow (nuclei). Particles that are too small are unstable and dissolve in the solution. The nucleation rate, J_N, is defined as the number of created nuclei per unit volume and per unit time. The formed nuclei are characterized by a so-called critical size. Typical critical size values are within the range 1–50 nm. The nucleation rate is a nonlinear increasing function of supersaturation. The nucleation stage in a precipitation process is often difficult to observe. If light is used as a probe to study precipitation, nuclei can be treated as Rayleigh scatterers. Considering the nuclei concentration, interaction between light and suspension is usually below the detector threshold. Other methods (for instance, small-angle X-ray scattering) are preferred, but are more difficult to apply. Details about the nuclei are not known. Hence, nuclei leading to inorganic particles are often considered as amorphous and spherical.

The following stage is the growth of the nuclei. They may additionally convert to crystals. Crystals present facets, the occurrence of which can be explained from crystallography and thermodynamics. However, depending on the precipitation reaction, only amorphous particles (i.e., hydroxylated compounds) can be found. Usually, the growth rate is defined as the derivative of crystal characteristic length (e.g., the diameter) with time. The growth rate increases with the supersaturation. Most often the relation between growth rate and supersaturation is linear.

For different reasons (one is the decrease of supersaturation during precipitation, due to the mass transfer from solution to crystals), an upper size limit for the growing crystals is observed. At the end of the second stage, crystal or particle size ranges between 0.1 and 10 μm. During this period, particles become large enough to scatter light effectively. Thus, light scattering methods are suitable for studying the growth of crystals or primary particles in suspension.

Before or after reaching the end of growth, crystals or amorphous particles can form clusters or agglomerates. Agglomeration requires the collision of particles and their subsequent adhesion due to attractive forces (for instance, van der Waals forces). Consolidation between primary particles or crystals can take place by crystalline growth from the contact point. In quiescent liquids, the particle collisions are due to their Brownian motion. For flowing suspensions, collisions are due to Brownian motion for small particles or crystals (smaller than about $0.2\,\mu$m) and to local shear for larger particles.

When the agglomerate increases in size, it becomes fragile. Then, break-up takes place and a limit size is reached (with values in the range $5–100\,\mu$m). The stress acting on the agglomerate results from the shear, but also the transition between viscous and inertial turbulent regimes. This often leads to agglomerates containing only a few primary particles (less than one hundred primary particles).

Summarizing: inorganic solutes can lead to solid particles in a batch precipitation vessel, provided that the solution is initially supersaturated. Nucleation, i.e. the birth of nuclei with a critical size, takes place, while supersaturation decreases as a consequence. Finally, supersaturation becomes too small, to produce new nuclei. Thus, there is a mass transfer from solution to the nuclei surface leading to the growth of nuclei. In this way, crystals or amorphous particles are formed. As supersaturation tends to one, growth stops. Depending on the surface charge of particles, their agglomeration may occur throughout the growth period.

2.2.2 Particle shapes during precipitation

Images from electron microscopy often show the complexity of particle structure. Particles formed by growth from solution can be crystals with well-defined crystalline faces, but may be agglomerates of smaller (nanometric) particles. In this case, agglomeration can be due to Brownian motion and the subsequent collision of particles, but also to the contact of specific crystalline faces belonging to two particles. The first situation leads to random agglomerate with spherical symmetry. The second phenomenon, also called orientated agglomeration, leads to regularly shaped particles (i.e., cylinders as disks stack). It must be underlined that the mechanism of orientated agglomeration is still being studied. Whatever the structure of particle, crystals, random or ordered agglomerate of nanoparticles, their geometric characteristics are easily determined by image analysis of electron micrographs.

However, these particles are rarely separate. They form agglomerates after collision due to Brownian motion and/or shear flow. The structure of agglomerates is disordered and is often considered as fractal-like. However, the reader must keep in mind that these agglomerates consist of only a few particles.

Fig. 2.1 presents agglomerates of $SrMoO_4$, strontium molybdate, crystals (Cameirao et al., 2008). They are obtained by precipitation:

$$SrCl_2 + Na_2MoO_4 \rightarrow SrMoO_4 + 2NaCl\,.$$
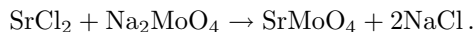
Bipyramidal crystals in the size range $3–10\,\mu$m are formed. Agglomerate size is in the range $20–80\,\mu$m.
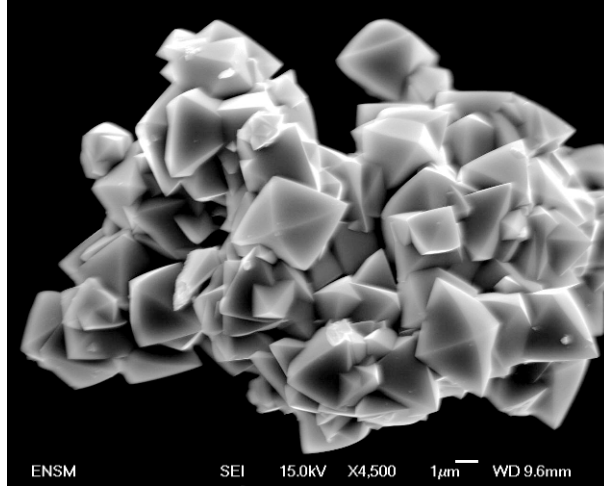
Fig. 2.1. Agglomerate of SrMoO$_4$ crystals.
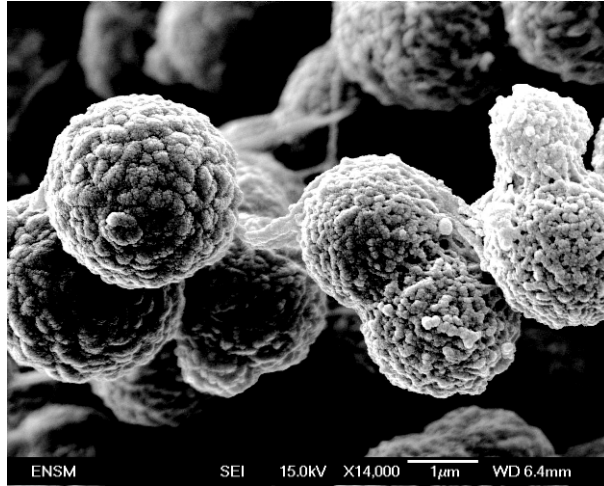
Fig. 2.2. Multi-scale ZnS agglomerate.

Fig. 2.2 presents agglomerates of zinc sulphide particles (Mekki-Berrada et al., 2005). They are obtained by homogeneous precipitation:

$$\mathrm{ZnSO_4 + CH_3CSNH_2 + 2H_2O} \xrightarrow[80^\circ C]{H^+} \mathrm{ZnS + CH_3CO_2H + NH_4^+ HSO_4^-} \ .$$
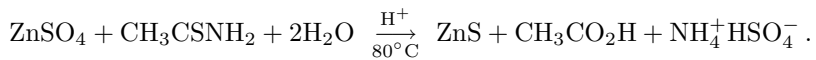
ZnS particles are sphere-like with a mean size equal to $3\,\mu$m. They consist of nanoparticles, $30\,$nm sized (one may observe an intermediate structure in the range $100\ldots300\,$nm). Micro-particles seem relatively dense. However, porosity and inner structure depend on the acidity and temperature. Micro-particles collide to form agglomerates in the range 20–60 μm.

Fig. 2.3 shows ordered agglomerates resulting from the stacking of $Ni(OH)_2$ nanosized disks (Coudun et al., 2007). They are obtained by precipitation from nickel di-dodecylsulfate and ammonia:

$$Ni(DS)_2 + 2OH^- \xrightarrow[60°C]{NH_3} Ni(OH)_2 + 2DS^- \,.$$

Fig. 2.3. $Ni(OH)_2$ nanosized agglomerates.

2.2.3 Dynamics of precipitation: modelling

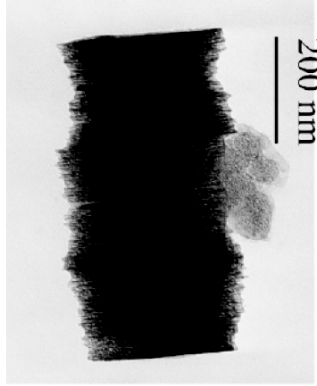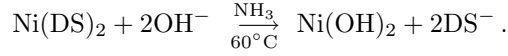In order to manage the complexity of precipitation dynamics, each particle in the precipitation reactor is characterized by space coordinates (x, y, z) and internal coordinates p_i (i.e. radius, characteristic lengths of crystal, volume, porosity, gyration radius, fractal dimension, ...) with $1 \leq i \leq P$.

The larger the number P, the more comprehensive the description of the particles. So, the population density function $n(x, y, z, p_1 \ldots p_P)$ is such that $dN = n\, dx\, dy\, dz\, dp_1 \ldots dp_P$ represents the number of particles with x in the range $[x; x + dx]$, p_i in the range $[p_i p_i + dp_i]$.

This population density obeys the population balance equation (PBE), that can be formally written as:

$$\frac{\partial n}{\partial t} = -\vec{\nabla} \cdot (\vec{v}n) - \sum_{i=1}^{P} \frac{\partial}{\partial p_i}(G_i(S)n) + J_N(S)\delta(p_1 - p_{1c}) \ldots \delta(p_P - p_{Pc}) + V_{ag} \,, \quad (2.1)$$

where $\vec{v}$ is the particle velocity, t is the time, G_i is the growth rate for the p_i parameter $[G_i = (dp_i/dt)]$, δ is the Dirac function, p_{ic} is the internal parameter corresponding to the critical nucleus, $J_N(S)$ is the nucleation rate as a function of the supersaturation S, and V_{ag} is the agglomeration rate.

More often, the following assumptions are used:

– homogeneous suspension
– only one internal parameter (particle radius)

– agglomeration taken into account only at the end of nucleation and growth
– fractal-like agglomerates with constant fractal dimension

For fractal-like agglomerates, the relation between the number j of primary particles inside the agglomerate and its outer radius R_j is:

$$R_j = a \left(\frac{j}{S_r} \right)^{1/D_F} , \qquad (2.2)$$

where a is the radius of the primary particle. D_F and S_r are respectively the fractal dimension and the structure factor, which is a function of D_F.

Attempts to consider two internal parameters (radius and length for particles such as a needle, solid volume and surface area for porous particles) have also been made (Tandon and Rosner, 1999; Kostoglou et al., 2006).

Summing up, precipitated particles have a multi-scale structure. One commonly observes three characteristic length values: $20\,\mathrm{nm}$, $2\,\mu\mathrm{m}$, $20\,\mu\mathrm{m}$. Sometimes, only two ($2\,\mu\mathrm{m}$, $20\,\mu\mathrm{m}$) are observed. The smallest particles are most often dense and spherical. The intermediate particles are relatively dense and have a well-defined shape (i.e. sphere, cylinder, ellipsoid, etc.). The largest scale corresponds to disordered or random agglomerates. The reader interested in details of precipitation and population balance may refer to Sugimoto (2000) and Randolph and Larson (1988).

2.2.4 Particle sizing during precipitation

Considerable efforts are made to understand the precipitation mechanisms and to predict the change of the particle morphology with time. On the other hand, industrialists need to monitor and control the precipitation process. Off-line size measurements (i.e. using filtration, powder drying and scanning electron microscope (SEM) observations or suspension sampling and sizing with granulometers) are now avoided because these operations modify the particle morphology. On-line measurements (i.e., using a recirculation loop with a measurement cell in a granulometer) are possible, but representative sampling is difficult to carry out. In-line measurements are preferred. They are often based on light extinction and are obtained from turbidimetric sensors. So, turbidimetry will be at the centre of this chapter.

Typically, the optical sensor for particle sizing is not the only one in the precipitating suspension. The temperature probe and concentration sensors are always introduced into it. Thus, supersaturation and solid fraction (via mass balancing from solute concentration) are deduced and, as a consequence, are known.

A turbidimetric sensor records the transmitted light intensity I_t. One defines the extinction coefficient or turbidity[1] as (see, for instance, Elimelech et al., 1995):

$$\tau = -\frac{1}{L} \ln \frac{I_t}{I_0} . \qquad (2.3)$$

___

[1]Definitions and notations in Eqs. (2.3)–(2.5) are used by researchers in the field of particle sizing concerning suspensions. Other researchers prefer these ones: $\tau^* = -\ln(I_t/I_0)$ and $\sigma_{ext}(\lambda) = \tau^*(\lambda)/L$ where τ^* and σ_{ext} are the optical thickness and the extinction coefficient, respectively.

I_0 and L are the incident light intensity and the geometrical thickness of the medium, respectively. For a monodisperse diluted suspension, the turbidity obeys the equation:

$$\tau(\lambda) = N(x_s, y_s, z_s, p_1 \ldots p_P) \, C_{ext}(\lambda, p_1 \ldots p_P) \qquad (2.4)$$

The functions N and C_{ext} are the particle number concentration and the extinction cross-section of the particles. (x_s, y_s, z_s) are the coordinates of the sensor in the reactor.

For a complex diluted suspension, turbidity contains the contribution of each kind of particles:

$$\tau(\lambda) = \int_{[p_1 \ldots p_P]} n(x_s, y_s, z_s, p_1 \ldots p_P) \, C_{ext}(\lambda_i p_1 \ldots p_P) \, dp_1 \ldots dp_P \, . \qquad (2.5)$$

Thus, the turbidity monitoring gives information on the population density change with time during the precipitation process.

Two strategies can be considered for the analysis of turbidity signals:

– inversion of the integral equation (Eq. (2.5)) in order to get the population density. Then, comparison to PBE (Eq. (2.1)) solution and identification of unknown physicochemical and morphological parameters (i.e., fractal dimension . . .)
– PBE (Eq. (2.1)) solving; calculation of $\tau(\lambda)$ (Eq. (2.5)); comparison with experimental turbidity for deducing the unknown physicochemical and morphological parameters

For numerical reasons, the last one is preferred. However, whatever the strategy, the knowledge of $C_{ext}(\lambda, p_1 \ldots p_P)$ is needed.

The extinction cross-section is dependent on the relative refractive index m, which is the ratio between the refractive indices of the material and the suspending medium. Three typical cases can be envisaged: low optical contrast m–1 value ($0 < m - 1 < 0.1$), moderate contrast m–1 value ($0.1 < m$–$1 < 0.5$) and high optical contrast m–1 value (m–$1 > 0.5$). Corresponding materials (suspended in water) could be, respectively, silica SiO_2 ($m = 1.08$), alumina Al_2O_3 ($m = 1.20$) and titania TiO_2 ($m = 2$).

We will focus our work on non-absorbing (in the visible range) materials that are most commonly found in the precipitation process. Thus, scattering C_{sca} and extinction C_{ext} cross-sections are equal.

It is obvious that PBE solving, cross-section calculation and optimization procedure require great computational efforts and make it difficult to get results in a short time. Therefore, any rapid calculation of the optical cross-sections would be a step forward. The accuracy of approximations has to fit the measurement accuracy. In the case of turbidity, measurements within 3% error can be considered as satisfactory.

The need for approximations is particularly important for agglomerates[2]. Fast calculations have to be based on known approximations coming from light scattering theory. The next section briefly recalls them.

2.3 Approximations for non-spherical particles

The scattering cross-section is a function of the dimensionless particle size parameter x ($= ka$ for a sphere), the particle and the medium optical refractive indices respectively denoted n_p and n_m, the wavelength λ (and the wave number $k = 2\pi/\lambda$) of the incident light in the medium and the orientation of the incident light in the relation of the particle position. The relative refractive index m, which is used in the following equations, is the ratio between the material refractive index n_p and the medium refractive index n_m.

The exact theory was developed for a sphere in 1908 by G. Mie (see van de Hulst, 1981) and for spheroids by several authors (Asano and Yamamoto, 1975; Asano, 1979; Asano and Sato, 1980; Voshchinnikov and Farafonov, 1992; Farafonov et al., 1999).

In this section, three classical approximations are recalled: the Rayleigh approximation, the Rayleigh–Gans–Debye approximation and the Anomalous Diffraction approximation. Principles are presented and an application is given for a sphere. The reader interested in details on scattering theories may refer to Van de Hulst (1981) and Kokhanovsky (2001).

2.3.1 Rayleigh approximation

The Rayleigh approximation that considers the scatterer as an oscillating dipole has a validity range of $x \ll 1$, $|mx| \ll 1$. So, the scattering efficiency factor for a sphere is:

$$Q_{sca} = \frac{8}{3} x^4 \left| \frac{m^2 - 1}{m^2 + 2} \right|^2 \tag{2.6}$$

and the scattering cross-section is $C_{sca} = Q_{sca}G$ (G represents the particle projected area, for a sphere $G = \pi a^2$).

A comparison between this approximation and the Mie exact theory shows that the validity range, in terms of maximum size, varies according to the relative refractive index and the scattering angle (Mishchenko et al., 2002, 2004).

2.3.2 Rayleigh–Gans–Debye approximation

The validity range of the Rayleigh–Gans–Debye approximation (RGD) is: $2x|m - 1| \ll 1$ and $|m - 1| \ll 1$.

---

[2]The term aggregation corresponds to the formation of a cluster, the primary particles of which only interact by physical forces such as van der Waals forces. On the other hand, agglomeration is aggregation followed by strengthening at the contact point in a supersaturated solution. Aggregate and agglomerate optical properties will be treated in the same way.

Fig. 2.4 represents a particle with an unspecified shape lit by a plane wave being propagated along the axis z'. It is supposed that each volume element is a Rayleigh scatterer and behaves independently of the other particle volume elements. The scattering waves of all these volume elements interfere. The phases of all these scattering waves are ascribed to a common coordinates reference in order to handle their amplitude.
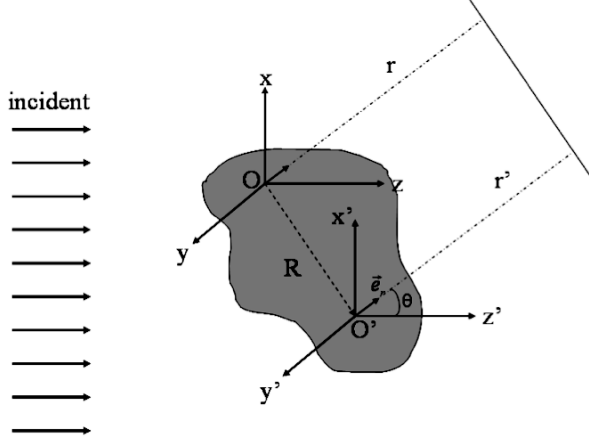

Fig. 2.4. RGD approximation.

The expression of the contribution, of the volume element ΔV located out of O, to the scattering field by the particle is:

$$\begin{pmatrix} \Delta E_{\parallel,sca} \\ \Delta E_{\perp,sca} \end{pmatrix} = \begin{pmatrix} S_2 & 0 \\ 0 & S_1 \end{pmatrix} \frac{e^{i \cdot k \cdot r - i \cdot k \cdot z}}{-i \cdot k \cdot r} \Delta V \begin{pmatrix} E_{\parallel,inc} \\ E_{\perp,inc} \end{pmatrix}.$$

The contribution of a volume element located in O' will be:

$$\begin{pmatrix} \Delta E_{\parallel,sca} \\ \Delta E_{\perp,sca} \end{pmatrix} = \begin{pmatrix} S_2 & 0 \\ 0 & S_1 \end{pmatrix} \frac{e^{i \cdot k (r - z)}}{-i \cdot k \cdot r} \Delta V \, e^{i\delta} \begin{pmatrix} E_{\parallel,inc} \\ E_{\perp,inc} \end{pmatrix}.$$

with $\delta = k\vec{R} \bullet (\vec{e}_z - \vec{e}_r)$ and $\vec{R} = \overrightarrow{OO'}$. S_1 and S_2 are the amplitude functions per volume unity:

$$S_1 \approx -\frac{ik^3}{2\pi}(m-1) \ \text{ and } \ S_2 \approx -\frac{ik^3}{2\pi}(m-1)\cos\theta\,.$$

θ is the scattering angle.

Integration is done with respect to particle volume V to obtain the total field in the direction $\vec{e}_r$. So, the amplitude functions for the particle are:

$$S_1 = -\frac{ik^3}{2\pi}(m-1)Vf \ \text{ and } \ S_2 = -\frac{ik^3}{2\pi}(m-1)Vf\cos\theta\,.$$

The form factor f obeys:

$$f = \frac{1}{V} \int_V e^{i\delta} \, dV \,, \tag{2.7}$$

that becomes for a sphere:

$$f(u) = \frac{3}{u^3}(\sin u - u \cos u), \quad u = 2x \sin \frac{\theta}{2} \,.$$

It follows for a spherical particle (Van de Hulst, 1981) that:

$$Q_{sca} = \int_0^\pi F(\theta) \, d/\theta(\pi a^2) \,, \tag{2.8a}$$

where,

$$F(\theta) = \pi a^2 \frac{4}{9} |m - 1|^2 x^4 f^2 \left(2x \sin \frac{\theta}{2}\right)(1 + \cos^2 \theta) \sin \theta \,. \tag{2.8b}$$

2.3.3 Anomalous Diffraction approximation

This approximation, due to Van de Hulst, bears the name of anomalous diffraction (AD) because, for low optical contrast, the light passing through the particle (transmitted without deflection) interferes with that diffracted, then producing a diffraction known as anomalous (Fig. 2.5).

Let us consider particles such as: $x \gg 1$ and $|m_r - 1| \ll 1$ (see the discussion of Videen and Chylek (1998) and Liu (1998)).

The second condition implies that the rays are not deviated when they cross the interface particle-medium and that the reflection is negligible with the same interface. Extinction is therefore due to:

– absorption of the light passing through the particles
– interferences between the light passing through the particle and that passing around it
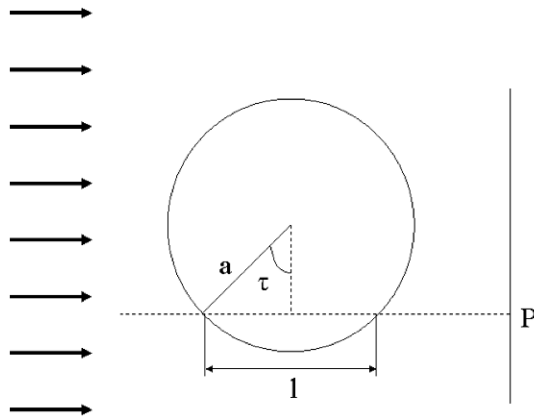

Fig. 2.5. Anomalous Diffraction approximation; *ray passing through a sphere.*

Following Van de Hulst (1981), one derives:

$$C_{ext} = \frac{4\pi}{k^2} \operatorname{Re}\{S(0)\} \text{ with } S(0) = \frac{k^2}{2\pi} \iint\limits_{[S_p]} (1 - e^{-ik(m-1)l}) \, dy \, dz \,.$$

Integration is performed over the particle projected area S_p on a plane perpendicular to the propagation direction. l is the computed path of light through the particle, which is a function of the projection coordinates x and y. The integrand represents the subtraction with 'the part of shade' (value 1) of the rays passing through the particle ($e^{-ik(m-1)l}$).

If m is real,

$$C_{sca} = 2 \iint\limits_{[S_p]} \left[1 - \cos(kl(m-1)) \right] dS_p \,. \tag{2.9}$$

Therefore, it follows for a sphere

$$Q_{sca} = Q_{ext} = 2 - \frac{4}{\rho} \sin\rho + \frac{4}{\rho^2}(1 - \cos\rho) \,, \tag{2.10}$$

where $\rho = 2x(m-1)$.

The anomalous diffraction was applied to a sphere and an infinitely long circular cylinder (Van de Hulst, 1981), a prism column (Chylek and Klett, 1991), a hexagonal crystal of ice (Sun and Fu, 1999), ellipsoids (Lopatin and Sid'ko, 1988; Streekstra and Hoekstra, 1994), a short cylinder (Liu et al., 1998) and other various forms (Sun and Fu, 2001; Yang et al., 2004).

A comparison between AD and the exact theory (Liu et al., 1998) suggests that AD estimates the extinction more precisely in the case of a random orientation of non-spherical particles than for spheres.

The next section treats approximations for the case of clusters of spheres. The derived approximations are directly related to the previous ones.

2.4 Approximations for aggregate scattering cross-section

This part begins with a short summary of the exact methods. It is followed by a study of the relation between aggregate scattering cross-section and physical characteristics. Finally, four approximations are described and an illustration in the field of precipitation is presented.

2.4.1 Exact theory for non-spherical particles and aggregates

The presented summary (see Table 2.1) of the different exact methods is not exhaustive. But we try to show several methods used to calculate the optical properties of an aggregate. We invite the reader to consult the article of Kahnert (2003) to have a more complete range of these methods and the papers series of Mishchenko et al. (2007, 2008). It is rather difficult to classify them precisely and especially to enumerate all of them. Nevertheless one can classify them in three main categories:

Table 2.1. Methods for treating the light scattering by a non-spherical particle or an aggregate (N is the number of operations in the algorithm (Kahnert, 2003))

Name	Principle	Applications	Strong and weak points
Methods based on partial derivative equations			
SVM Separation of Variable Method	Method applied in the case of the Mie theory; it can be applied when the boundary of the considered particle coincides with the reference frame.	In any reference frame, where the variables separation can be applied. Asano and Yamamoto (1975) used this technique to determine the optical properties of a spheroid.	– The solution obtained is known as exact but calculations are long – the operation for each orientation must be repeated – $N \approx O(x^3)$
FDTD Finite Differences Time Domain	This method consists of discretizing the Maxwell equations, in space and time. Then to solve them it is necessary to start from the initial values (Yang and Liou, 2000).	All particle shapes.	– the operation for each orientation must be repeated – $N \approx O(x^4)$
FEM Finite Element Method	This method consists in discretizing the Helmholtz equation in space and solving numerically using the boundary conditions (Coccioli et al., 1996).	All particle shapes.	– the operation for each orientation must be repeated – the precision depends on the grid which must be selected according to the particle shapes – $N \approx O(x^7)$
PMM Point-Matching Method	In this method, the internal and external fields are expressed as a spherical harmonic vector. The tangential field at the boundary of a particle must be continuous for a fixed number of points belonging to the particle surface.	Normally all particle shapes, but problems are known for the elongated geometries.	– this method is limited to the quasi-spherical particles, it has a dubious convergence, and thus, requires a long CPU time (Wriedt, 1998).

Table 2.1. (Continued)

Name	Principle	Applications	Strong and weak points
Volume or surface integration			
VIEM Volume Integral Equation Method	The field inside and outside the volume is expressed in terms of incident and internal fields for the selected volume. – the internal field is evaluated by considering, for each volume element, as being constant: MOM (Method of Moments) (Harrington, 1968). Alternatively, – each element is regarded as a dipole: DDA (Discrete Dipole Approximation) (Draine and Flatau, 1994)	Inhomogeneous, anisotropic particles.	– MOM and DDA have a long CPU time – the operation for each orientation must be repeated – $N \approx O(x^9)$

1. Methods based on the partial derivative equations which calculate the scattering field by solving the Maxwell equations or the Helmholtz equation. They are subjected to the boundary conditions suitable in the time or the frequency domain.
2. Methods based on integration over volume or surface of equations derived from the Maxwell equations. Thus, the boundary conditions are automatically included in the solution.
3. The other methods are known as hybrids since they derive from the various approaches.

It is important to specify the meaning of the 'T-matrix method' expression which is found in a lot of publications. In the T-matrix method, the incident and scattering fields are expressed in the form of a series of spherical vector wave functions. This approach is named the T-matrix method when the expansion coefficients of the incident wave and the scattering wave are connected by a linear transformation (T is for transition). This matrix T contains all the information on the particle's optical properties for a given wavelength. It is a function of the size parameter, the shape, and the optical refractive index of the considered particles, but it does not depend on the incident field. Thus this matrix is not to be computed at each particle orientation change or change of the incident wave direction.

To classify the publications set relying on this method, a database review was carried out by Mishchenko et al. (2004, 2007, 2008). This method is, in fact, a technique of calculation, which is found associated with various methods (e.g., SVM). Thus, any method making it possible to formulate the problem in the way of a matrix T is called the T-matrix method.

The solving by separation of variables (SVM) for only one sphere can be enlarged to an aggregate of spheres by using the translation theorem for the spherical wave vector functions which expresses them in various bases of coordinates, and, by applying a superposition principle. The total scattering field for an aggregate is then represented by the superposition of the individual scattering fields resulting from each particle in the knowledge that these fields are interdependent. Moreover, one can formulate the problem as a T-matrix. This method is very precise but its computation time depends on the number and the size parameter of primary particles.

We will use in the continuation of this text a method which is in fact a particular case of the T-matrix method (Mishchenko et al., 2004) bearing the name of GMM (Generalized Multi-particle Mie-solution).

We did not find a comparison of the various methods, except for an article of Hovenier et al. (1996) which compared the T-matrix (method by surface integration), SVM and DDA. This article shows that the last is not completely in agreement with the two other methods. As no study was undertaken in this direction, the work presented in this article is achieved with a method which seems, closest to the one used for a simple sphere and validated by experiment (Xu and Gustafson, 2001): GMM. The details of GMM are given by Xu (1995, 1996, 1997a,b, 1998a).

2.4.2 Main features of the scattering properties of aggregates

We present a summary of the main features of the scattering properties of aggregates. Results come from the calculated optical properties of aggregates such as:

– aggregates of spherical primary particles
– number of primary particles in the aggregate $N \in [1, 100]$
– primary particle size parameter (x) in the range: $[0.013, 9.25]$.
– three different materials (SiO_2, Al_2O_3, TiO_2); non-absorbing materials

Optical properties are calculated by using GMM theory.

First of all it is interesting to study the effect of the inter-particle distance on the scattering cross-section.

2.4.2.1 The case of a two-sphere set

The evolution of the scattering cross-section of a two-sphere set according to the type of material, their size parameter and the center to center distance has already been studied by Mishchenko et al. (1995) and Quirantes et al. (2001).

The K_{Xu} parameter for different materials was used. K_{Xu} is defined as the ratio between the scattering cross-section of an aggregate and the sum of scattering cross-sections of N primary particles which form this aggregate (so, the denominator assumes non-interacting and non-interfering spheres).

$$K_{Xu} = \frac{C_{Xu,N}}{N C_{Mie,1}} \, . \tag{2.11}$$

The two spheres, denoted i and j, were gradually separated (center to center) by a factor F_{ij} proportional to their diameter, until they did not interact any more (K_{Xu} is equal to 1). As the separation distance is denoted d_{ij}, the factor obeys the relation:

$$F_{ij} = d_{ij}/(2a),$$

where a is the radius of the primary particle.

According to Fig. 2.6, for size parameter smaller than 0.5, the smaller the primary particle is, the greater the distance factor must be to obviate any interaction. We therefore endorse the conclusion of Kolokolova and Gustafson (2001): a suspension consisting of Rayleigh scatterers as primary particles has to have a very weak volume fraction to avoid multiple scattering, whatever the relative refractive index.

Interaction between particles cannot be ignored even if $F_{ij} > 4$ (for the whole range of the size parameter).

For spheres in contact, K_{Xu} (Fig. 2.6) increases with decreasing size parameter up to a value close to 2. When the two spheres are large enough, the deviation from the non-interacting limit is negligible (e.g., $K_{Xu} < 1.1$ for $x > 5$).

It therefore appears useful to evaluate the critical inter-particle distance for which interaction is negligible. An approximate method for aggregate optics calculation could take it into account.

2.4.2.2 The case of aggregate ($N > 2$)

Auger et al. (2003) studied the relation between the extinction cross-section of an aggregate, its shape (linear or compact configuration) and the number of primary particles (2, 4, 8, 13) in the case of titania TiO_2 (the optical refractive index being equal to 2.8). In this article, the average extinction cross-section (average on the polarization and the incident wave direction) divided by the aggregate volume (made up of monosized spheres) is calculated, according to their particle radius (between $0.04\,\mu m$ and $0.132\,\mu m$). It is found that there exist two size ranges (for $\lambda = 0.546\,\mu m$). For a primary particle radius smaller than $0.08\,\mu m$–$0.09\,\mu m$, an isolated primary particle scatters less than if it was contained in an aggregate. Primary particles belonging to the second range behave in an opposite way. They show that there exist two size ranges concerning the effect of aggregate shape: in the first range, a compact configuration scatters more than linear configuration, and conversely for the second range. Lastly, a comparison with the equivalent sphere approximation shows that the latter is not suitable. Auger et al. (2005) and Jacquier and Gruy (2007a) perform similar studies in the way that they compare the scattering cross-section for various configurations. The Auger et al. (2005) study is based on the distribution of randomly generated aggregates by classical mechanisms of aggregation.

Jacquier (2006) and Jacquier and Gruy (2007a) enlarged the study using different optical refractive indices, a greater range of the primary particle size parameter, and different configurations. They noted the effect of the primary particle number and the aggregate morphology. The results are summarized in the two next paragraphs.
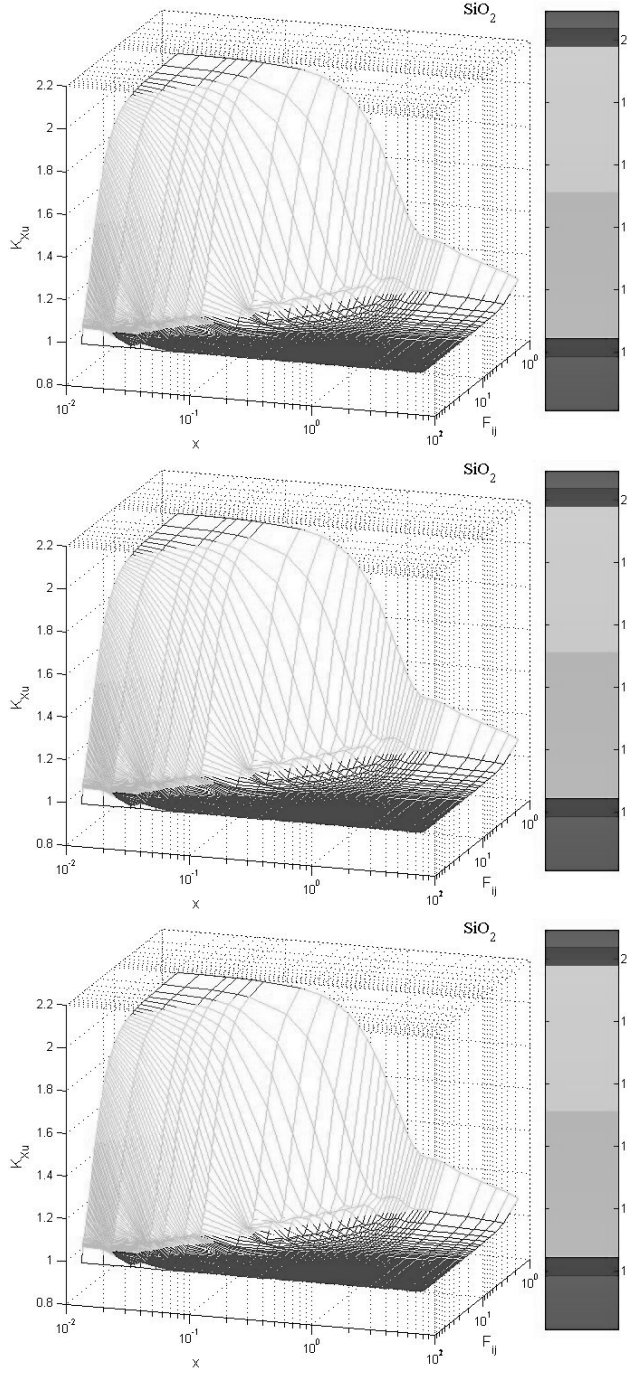
Fig. 2.6. Evolution of K_{Xu} according to the size parameter and the distance factor ranging between 1 and 100 for the three materials (SiO$_2$, Al$_2$O$_3$, TiO$_2$).

• *Effect of the number of primary particles on the scattering cross-section*
In the paper of Jacquier and Gruy (2007a), two extreme configurations were compared (linear and compact configuration). For each configuration, Jacquier and Gruy noticed that there exist two ranges. The first is for K_{Xu} larger than 2, and the second is for K_{Xu} ranging between 0 and 2. The value of the size parameter of the primary particles corresponding to the range boundary is a weak function of the optical refractive index, the primary particle number and the configuration. However, the authors suggest the first range for $x \in [0, 2]$ (Fig. 2.7(a)) and the second one for $x \in [2, 10]$ (Fig. 2.7(b)) (the limit of their study is for a size parameter smaller than 10). They conclude (as shown in Fig. 2.7):
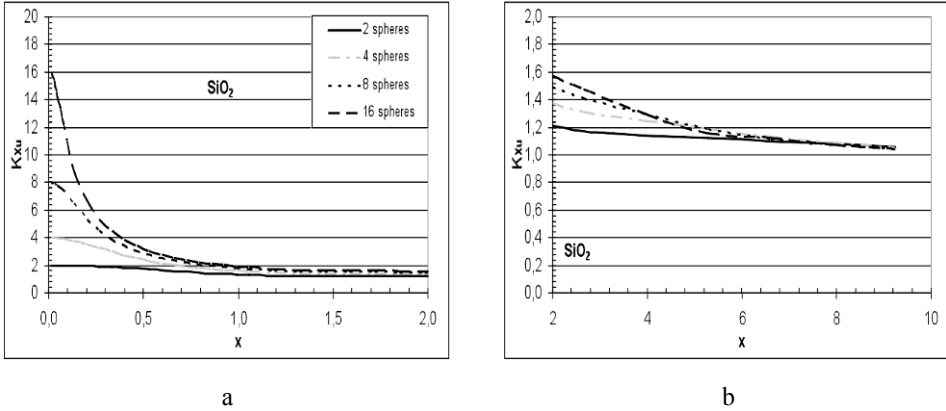

a   b

Fig. 2.7. K_{Xu} as a function of the size parameter for the linear configuration with N primary particles (2, 4, 8, 16) and for SiO₂ (Jacquier and Gruy, 2007a): (a) for the range $x \in [0, 2]$ and (b) $x \in [2, 10]$.

– for $x \in [0, 2]$, the larger the number of primary particles, the larger the scattering cross-section whatever the configuration. Indeed, in the case of very small size parameter, the aggregate scattering cross-section is proportional to the particle number square and to the primary particle scattering cross-section ($C_{Xu,N} \propto N^2 C_{Mie,1}$). This relation is checked on a lesser scale by aggregates with high refractive index (e.g., TiO₂). In addition the decrease of $K_{Xu}(x)$ seems to depend on the configuration.
– for $x \in [2, 10]$, $K_{Xu}(x)$ is not yet equal to 1 (Fig. 2.7(b)), i.e. the aggregate scattering cross-section is not the sum of the scattering cross-sections of each primary particle.

• *Effect of the aggregate morphology on scattering cross-section*
As illustrated in Fig. 2.8, it is possible to establish a classification of the configurations according to their scattering cross-section. In the x-domain, where $K_{Xu} > 1$, the scattering cross-section of the compact configuration is higher than that of the plane configuration, itself higher than that of p1 and p2 configurations (which are
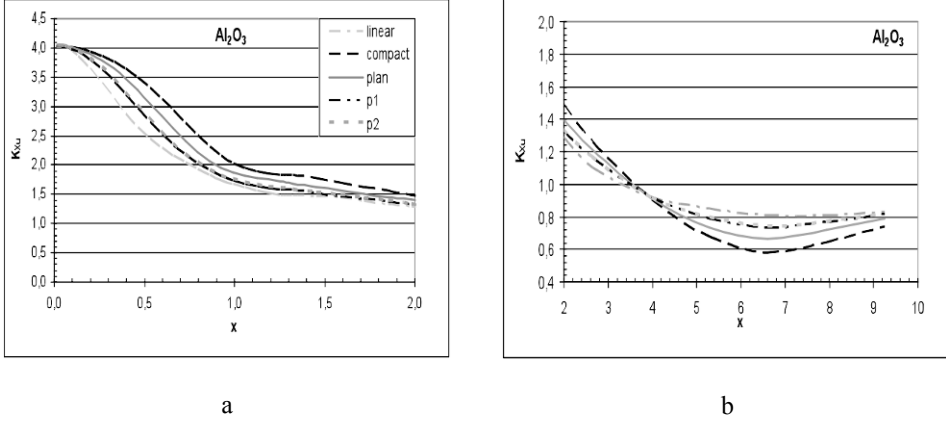
a   b

Fig. 2.8. K_{Xu} as a function of the size parameter for aggregates with four primary particles (linear, compact, plan, p1, p2) for Al_2O_3.

very close Fig. 2.9). The linear configuration is the weakest. The order is reversed for the other x-domain ($K_{Xu} < 1$). Thus, there are two extreme configurations, linear and compact, between which are other configurations.

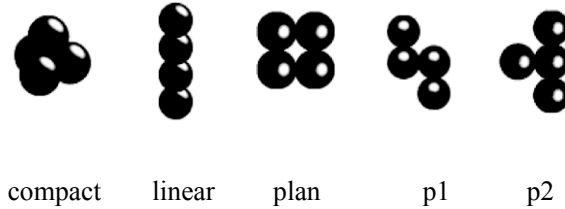compact   linear   plan   p1   p2

Fig. 2.9. Different aggregate configurations in the case of four primary particles.

The primary particles arrangement, i.e. the aggregate configuration, is not without effect on the scattering cross-section, nevertheless, the number of primary particles in it is the prevailing parameter in the range $x \in [0; 2]$. In the second range ($x \in [2; 10]$), the configuration is more important than the number of primary particles.

2.4.2.3 Conclusion on aggregate scattering cross-section

The study of scattering (C_{sca}) cross-sections of aggregates obtained with the exact method revealed that:

- the distance between particles is a relevant parameter for C_{sca},
- different aggregate configurations, following its shape or the number of primary particles which it contains, are perfectly distinguishable,
- the number of primary particles is the relevant parameter in the case of small size parameter x ($x \to 0$, $C_{Xu,N} \propto N^2 C_{Mie,1}$),

– there exists, for an aggregate with a given number of primary particles, two extreme configurations (linear and compact) between which the cross-sections of the others are located.

2.4.3 Approximate methods (CS, BPK, AD, ERI) for aggregates

In this subsection, we describe different approximate methods: the Compact Sphere method (CS), the Berry–Percival–Khlebtsov method (BPK), the Anomalous Diffraction method (AD), and the Effective Refractive Index method (ERI). A first comparison between these four methods was published by Gruy (2001) in connection with aggregation of SiO_2 micro-particles in water.

The study of the parameters influencing the optical properties of aggregate began with Fuller and Kattawar (1988a, b). Rouleau (1996) compared several approximate methods for optical properties based on:

– RGD approximation
– Non-interacting spheres
– Equivalent volume sphere
– Equivalent projected area sphere

This study was carried out only for compact aggregates with 30 primary particles whose size parameter was smaller than 0.6 and the refractive index was kept constant ($m = 1.7 + 0.1i$). He concluded that the abovementioned methods are not efficient except the one using the projected area.

The differences between the methods quoted in the next paragraphs are evaluated in Table 2.2. We chose to differentiate porosity and arrangement. The validity range of all these methods is normally the whole size parameter range except for AD, which, as already mentioned in subsection 2.3.3, is to be used only in the case of large particles.

Table 2.2. Comparison of approximate methods

Method	Does it take into account:		Does it use:
	the arrangement?	the interactions?	Maxwell–Garnett equation? (porosity)
CS	no	no	no
ERI	yes	no	yes
BPK	yes	yes	no
AD	yes	yes	no

In the next subsections, scattering cross-section values from the approximate method ($C_{method,N}$) and the exact method ($C_{Xu,N}$) will be compared. Then, the ratio K_m is defined as:

$$K_m = \frac{C_{method,N}}{C_{Xu,N}} \tag{2.12}$$

2.4.3.1 The Compact Sphere (CS) method

This method has to be mentioned because it is used as the first coarse approximation by investigators and by particle sizer manufacturers. One finds it under the name of equivalent sphere (in volume), and it will be compared with the other methods.
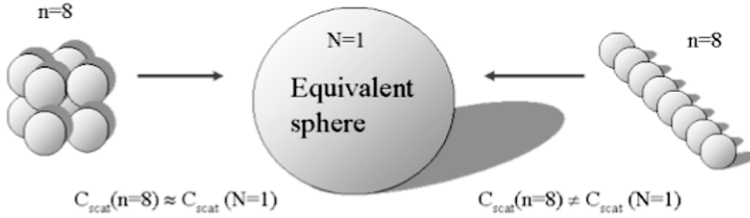

Fig. 2.10. The Compact Sphere method.

The aggregate is regarded as a full sphere, i.e. containing all the matter (Fig. 2.10). This method can be valid for aggregates of high compactness. The scattering cross-section $C_{CS,N}$ is then evaluated with the theory of Mie.

As shown in Fig. 2.11, the CS method overestimates the scattering cross-section for $x < 7$, whatever the configuration. As we will see in subsection 2.4.3.3, an aggregate can be considered as a (porous) sphere with an effective refractive index. Whatever the chosen equivalent sphere, the value of the scattering cross-section calculated by Mie theory is always smaller than the one obtained from the CS method. Moreover, this method does not take into account the interactions (interference and interaction).
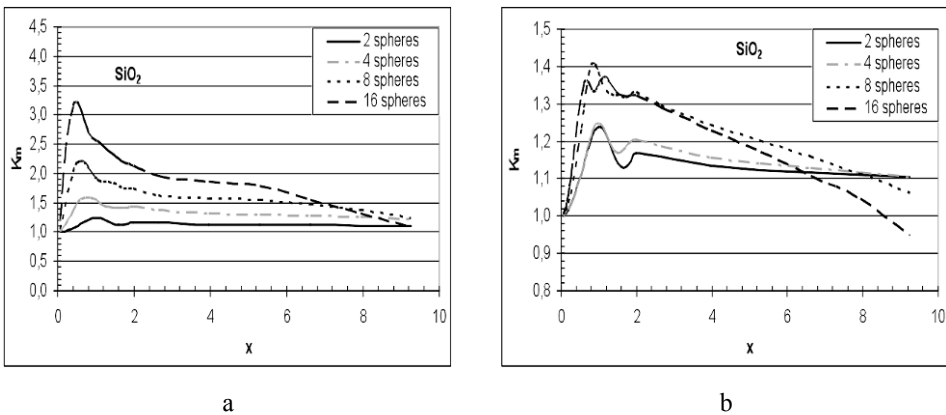

a   b

Fig. 2.11. The Compact Sphere approximation: K_m as function of the size parameter for SiO_2 (a) linear configuration, (b) compact configuration.

2.4.3.2 The Berry–Percival–Khlebtsov (BPK) method

This method originates from the work of Berry and Percival (1986) and Khlebtsov (1996). The three following points constitute the stages of the BPK method.

Step 1: Evaluation of the angular contribution of each primary particle to the scattering cross-section:

$$F_1(\theta) = \frac{C_{Mie,1}}{C_{RGD,1}} F(\theta) \,, \tag{2.13}$$

where $F(\theta)$ comes from the RGD approximation for a sphere (see Eq. (2.8b)). $F_1(\theta)$ is the corrected function for $F(\theta)$ in order to verify: $\int_0^\pi F_1(\theta)\, d\theta = C_{Mie,1}$.

Step 2: Calculation of the interferences of scattering waves for each pair of primary particles leading to a structure factor S which does not depend on polarization. The structure factor is related to the aggregate morphology through the inter-particle distances.

$$S(\theta) = \left[N + \sum_{i=j=1, i\neq j}^{N} R_{ij}(\theta) \right] \Big/ N^2 \,, \tag{2.14a}$$

where

$$R_{ij}(\theta) = \frac{\sin\left(2kd_{ij}\sin\left(\dfrac{\theta}{2}\right)\right)}{2kd_{ij}\sin\left(\dfrac{\theta}{2}\right)} \tag{2.14b}$$

and d_{ij} is the distance between i and j particles.

Step 3: Use of a corrective coefficient d taking into account the multiple scattering (Berry and Percival, 1986)

$$d^{-1} = \left[1 - \frac{3}{2N}(-a_{i1}p_r - a_{r1}p_i) \right]^2 + \left[\frac{3}{2N}(a_{r1}p_r - a_{i1}p_i) \right]^2 \,, \tag{2.15}$$

with

a_{r1} and a_{i1} are the real and imaginary parts of the first Mie coefficient a_1

$$p_r = 2 \sum_{j>i, i=1}^{N} p_{r1}(kd_{ij})$$

$$p_i = 2 \sum_{j>i, i=1}^{N} p_{i1}(kd_{ij})$$

$$p_{r1}(x) = \big(\cos x \, f_1(x) - \sin x \, f_2(x) \big)/x^2$$

$$p_{i1}(x) = \big(\sin x \, f_1(x) + \cos x \, f_2(x) \big)/x^2$$

$$f_1(x) = \sin x - \frac{x}{3} f(x) + \frac{1}{x}\left(f(x) - \frac{\sin x}{x} \right)$$

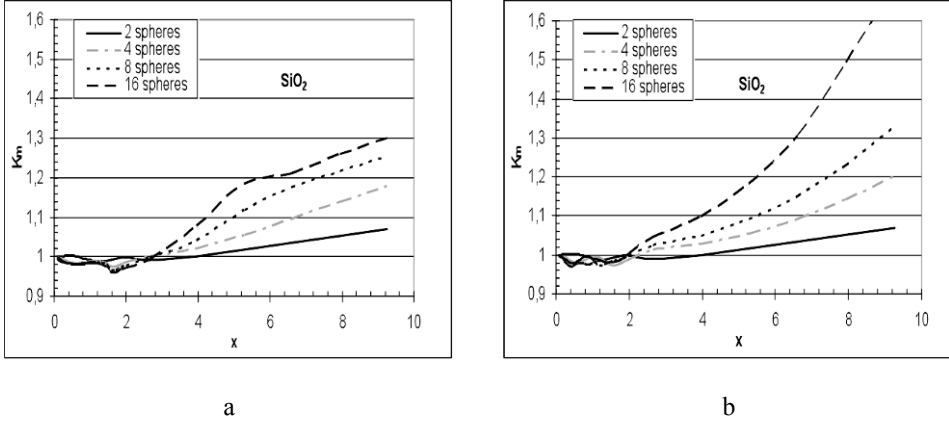a   b

Fig. 2.12. The BPK approximation: K_m as function of the size parameter for SiO$_2$ (a) linear configuration, (b) compact configuration.

$$f_2(x) = \frac{\sin x}{x} - f(x)$$

$$f(x) = \frac{3}{x^3}(\sin x - x \cos x)$$

Conclusion of steps:

$$C_{BPK,N} = N^2 d \int_0^\pi F_1(\theta) S(\theta) \, d\theta \qquad (2.16)$$

Fig. 2.12 shows that the BPK method is a satisfactory approximation of the exact method for the small size parameter ($x < 2$). The BPK method leads to an error smaller than 10% for a size parameter ranging between 0 and 2 in the case of SiO$_2$ and of Al$_2$O$_3$. For higher refractive index (i.e. TiO$_2$), the error increases until it reaches 30% (for more restricted size parameter range [0; 1]). The BPK method shows that the pair interactions must be taken into account only for small size parameters; their contribution in scattering cross-section calculation is less in the case of large aggregated primary particles.

2.4.3.3 The Effective Refractive Index (ERI) method

We have shown in subsection 2.4.2.2, that the location of the primary particles inside an aggregate and its shape had an effect on the scattering cross-section. The effective refractive index (ERI) method considers the shape. Knowing that the projected area of the scattering body (on the plane $(\vec{E}, \vec{H})$ of the incident wave) is a relevant parameter in optics, we consider an equivalent sphere starting from the aggregate projected area (Fig. 2.13).

Projection is carried out according to several successive planes (plane perpendicular to the incident wave vector). This corresponds to random rotation that takes place in a real situation (for instance, aggregate in a turbulent flow). Then, an average projected area $\langle S_p \rangle_0$ is calculated and an equivalent projected area
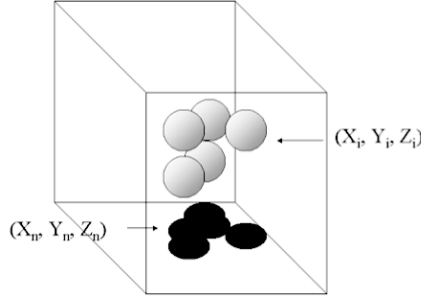
Fig. 2.13. Projected area representation.

sphere is defined. Successively, it can be deduced, the equivalent radius $a_{N,e}$, the solid volume fraction inside the sphere $\overline{\phi}_a = (Na_1^3)/a_{N,e}^3$, the effective refractive index m_a using the Maxwell–Garnett theory

$$\frac{m_a^2 - 1}{m_a^2 + 2} = \overline{\phi}_a \frac{m^2 - 1}{m^2 + 2},$$

and then the extinction cross-section $C_{ERI,N}$ by means of Mie theory. This method is more efficient than the other equivalent sphere methods, because the solid volume fraction in this sphere is always high $(0.1 < \overline{\phi}_a < 1)$.

ERI method behaves differently according to the configuration for small size parameter (Fig. 2.14). Indeed, Csca value calculated with this method is higher than the scattering cross-section calculated with the exact method for a linear configuration (Fig. 2.14(a)). This deviation can be taken in consideration and calculation has to be corrected in order to reduce the deviation between ERI and exact methods.

Jacquier and Gruy (2007a, b) proposed a corrective factor $F(x, d_1/a)$ for the scattering cross-section $C_{ERI,N}$. This is written as:

$$C_{ERI,N}^{corr} = C_{ERI,N}/F(x, d_1/a), \tag{2.17}$$

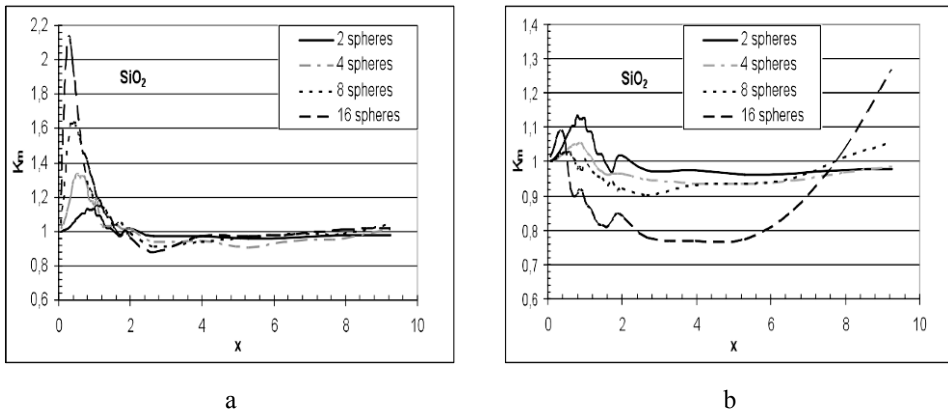a   b

Fig. 2.14. The ERI approximation: K_m as function of the size parameter for SiO_2 (a) linear configuration, (b) compact configuration.

where d_1 is a morphological parameter defined as:

$$d_1 = \frac{1}{N(N-1)} \sum_{i,j} d_{ij} \tag{2.18}$$

2.4.3.4 The Anomalous Diffraction (AD) method

In subsection 2.4.2.2 it has been already mentioned that morphology becomes more important for large size parameters. The anomalous diffraction approximation, clarified in subsection 2.3.3 (Van de Hulst, 1981), accounts for the aggregate morphology by means of the intercept (chord) of a light ray and the aggregate (Fig. 2.15).
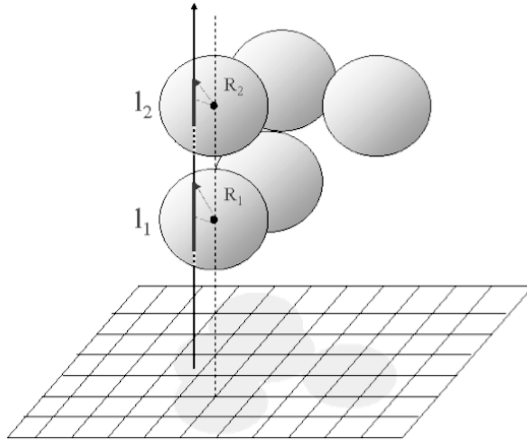

Fig. 2.15. Definition of a chord.

The various possible chords $l_1, l_2 \ldots$ were evaluated and introduced as $l = \sum_i l_i$ into Eq. (2.19)

$$C_{AD,N} = 2 \iint\limits_{[S_p]} \left(1 - \cos \frac{2\pi}{\lambda} l(m-1)\right) dy\, dz = 2 \iint\limits_{[S_p]} \left(1 - \cos x(l/a)(m-1)\right) dy\, dz \,.$$

$$\tag{2.19}$$

$[S_p]$ is the projection plane. Details or examples on expressions relating l/a and (y, z) can be found in Yang et al. (2004) and Gruy and Jacquier (2008).

This calculation is repeated while rotating the aggregate or changing the projection plane. So, a mean value of scattering cross-section is deduced (Fig. 2.16). As expected, the AD method is not suitable for small size parameters but proves to be a good approximation for a size parameter higher than 2. It is important to recall that AD is strongly related to the configuration (morphology) since it includes in its formulation the chord length distribution of the aggregate.
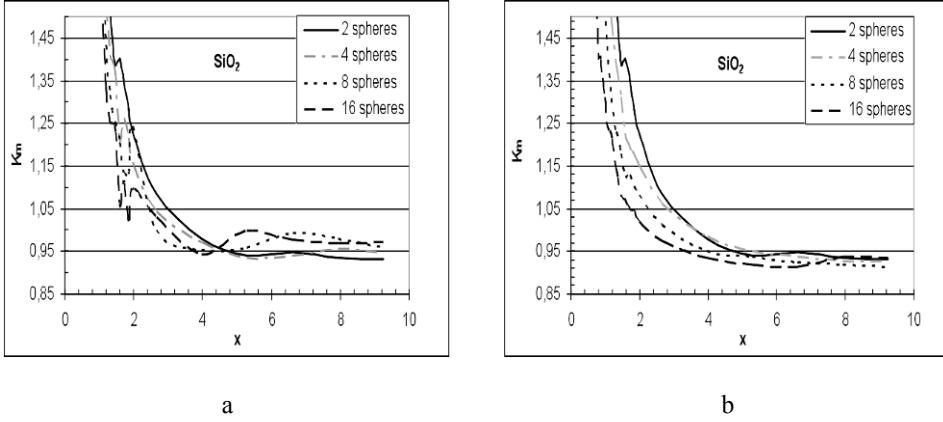
a   b

Fig. 2.16. The AD approximation: K_m as function of the size parameter for SiO_2 (a) linear configuration, (b) compact configuration.

2.4.3.5 Summary

Approximate methods facilitate the estimation of the aggregate scattering cross-section in a short computation time. Jacquier and Gruy (2007a) evaluated the performance of these four approximate methods with respect to the exact method:

–   Methods replacing an aggregate by a compact sphere (CS) are inappropriate.
–   The BPK (Berry–Percival–Khlebtsov) method is valid for $0 < x < 2$ with an error which increases with the material refractive index.
–   The corrected ERI (Effective Refractive Index) method is the approximate method capable of efficiency over all size parameters. The error for a scattering cross-section is always smaller than 5%.
–   The AD (Anomalous Diffraction) method works fairly well for $2 < x < 10$ and is less sensitive to refractive index variation.

2.4.4 Application: turbidity versus time during the agglomeration process

As mentioned in section 2.2, nucleation and growth lead to (primary) particles with a size between $0.1\,\mu m$ and $10\,\mu m$. Then, these particles collide and agglomerate by Brownian motion and/or local shear. So, let us consider agglomeration of small monosized primary particles in a homogeneous suspension. Agglomeration proceeds as a bimolecular reaction, the kinetic constant of which can be expressed in terms of known quantities. Generally, the kinetic constant is a function of the sizes of the two colliding particles. However, in the case of Brownian agglomeration or shear agglomeration (but not for shear aggregation, i.e without consolidation of the particle cluster), the kinetic constant K_{ag} weakly depends on the particle size, so that we may consider it as not dependent on particle size. Following Kruyt (1952), modeling of agglomeration with constant K_{ag} leads to simple expressions for number concentrations in the agglomerate:

$$N_j = N_0(t/t_c)^{j-1}(1 + t/t_c)^{-j-1}\,. \tag{2.20a}$$

N_j is the number concentration in agglomerate consisting of j primary particles. N_0 is the number concentration in primary particles at time $t = 0$. There is no agglomerate at $t = 0$. t_c is the characteristic time of agglomeration. It obeys:

$$t_c = 2/(K_{ag}N_0)\,. \tag{2.20b}$$

For instance, $t_c = 3\mu/(4kTN_0\alpha)$ for Brownian agglomeration. T, k and μ are the temperature, the Boltzmann constant and the dynamic viscosity, respectively. α is a non-dimensional parameter representing the agglomeration efficiency ($0 < \alpha < 1$). For the sake of simplicity, we consider this parameter as a constant throughout the agglomeration process.

It will be pointed out that t_c and then N_j do not depend on the agglomerate morphology. The previous expressions are approximate, but are considered as a first and realistic approach to agglomeration dynamics.

At a given time, the turbidity of the suspension contains the contribution of each j-agglomerate:

$$\tau(\lambda, t) = \sum_{j=0}^{\infty} N_j(p_1^j \ldots p_p^j, t)C_{ext}(\lambda, m, p_1^j \ldots p_p^j)\,. \tag{2.21}$$

Following the ERI method, the internal coordinates relevant for scattering cross-section are a (the primary particle radius), j, $\langle S_p \rangle_0$. Even if the characteristic time does not depend on the morphology, it appears that large agglomerates have a fractal-like structure. Depending on the agglomeration mechanism, simulations give values of fractal dimension between 1.8 and 2.6. Due to restructuring of agglomerates, the fractal dimension is larger than 2. As the fractal dimension is larger than 2, the outer radius of the agglomerate is equal to the radius $a_{S,j}$ of the 'projected area' equivalent sphere. Small agglomerates do not have the fractal-like structure. However, we have shown (Gruy, 2001) that they can be described by means of a power law relating $a_{S,j}$ and j:

$$\frac{a_{S,j}}{a} = \left(\frac{\langle S_p \rangle_0}{\pi a^2} \right)^{1/2} = \left(\frac{j}{S_r} \right)^{1/D_F}\,. \tag{2.22}$$

Later on, we will consider Eq. (2.22) suitable for a wide range of primary particle numbers. Then,

$$\tau(\lambda, t) = \sum_{j=0}^{\infty} N_j(t, t_c)C_{ext}(\lambda, m, j, a, D_F)\,. \tag{2.23}$$

Figs 2.17 and 2.18 represent the change of turbidity (normalized by $\tau_0(\lambda) = N_0C_{ext}(\lambda, m, a)$) with time (normalized by t_c) for agglomeration of silica ($m = 1.08$). Figs 2.17 and 2.18 show the effect of two fractal dimensions ($D_F = 2.1$; $D_F = 2.5$) and two primary particle radii ($a = 0.1\,\mu$m; $a = 1\,\mu$m) respectively at $\lambda = 0.4\,\mu$m and $\lambda = 0.8\,\mu$m.
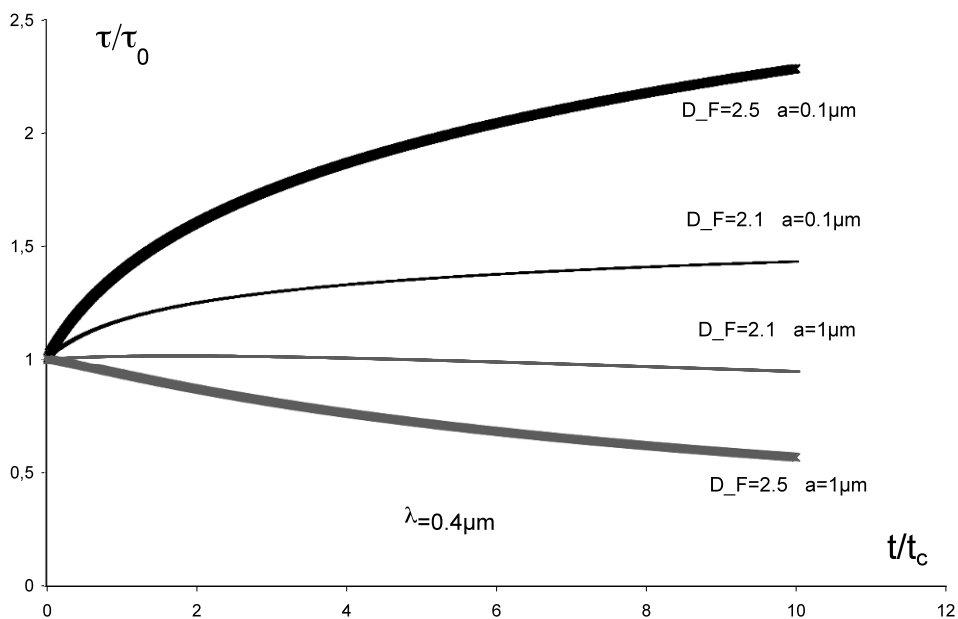
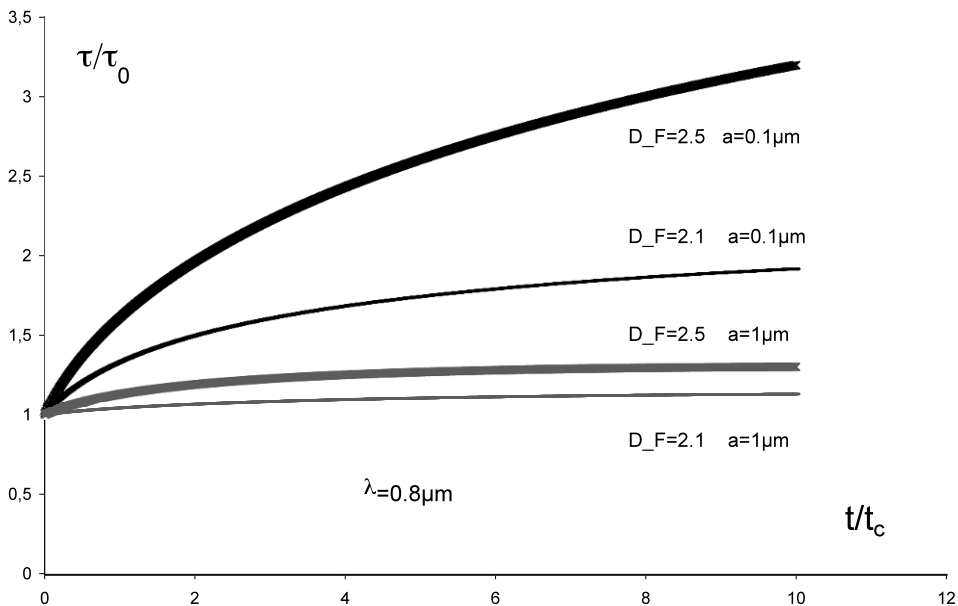**Fig. 2.17.** Normalized turbidity versus time; agglomeration of silica in water; $\lambda = 0.4\,\mu$m.

Fig. 2.18. Normalized turbidity versus time; agglomeration of silica in water; $\lambda = 0.8\,\mu$m.

2.5 Approximation for radiation pressure cross-section

2.5.1 Introduction

Often, precipitation leads to concentrated suspensions. On the one hand, transmitted light intensity becomes very weak making backscattering sensors more suitable than turbidimetric ones. On the other hand, multiple scattering takes place. Whatever the considered signal (backscattered, side-scattered or transmitted light), the interpretation has to account for multiple scattering. The most popular theory which considers this phenomenon is the radiative transfer theory, particularly its diffusion approximation (Ishimaru, 1978). The relevant phenomena associated with backscattering measurement are either coherent or incoherent ones. The first type result from interference caused by the double passage of the wave through the same particle (Tsang and Ishimaru, 1984, 1985; Wolf et al., 1988; Akkermans et al., 1988; de Wolf, 1991; Helfenstein et al., 1997). The angular width of the measured intensity peak is proportional to the transport mean free path $L_{tr} = (NC_{pr})^{-1}$, where N is the particle number concentration and C_{pr} is the radiation pressure cross-section. The second type only considers the multiple scattering: scattered light intensity is also a function of the transport mean free path. Theoretical calculations were compared to on- (off-) line experimental data for transmittance (Ishimaru et al., 1983) and retroreflectance (Kuga and Ishimaru, 1984; Nichols et al., 1997) experiments with suspensions of spherical beads, and a fairly good agreement between both was found.

The radiation pressure cross-section is expressed as a function of the extinction and scattering cross-sections, and also the asymmetry parameter ($g = \langle \cos\theta \rangle$):

$$C_{pr} = C_{ext} - C_{sca} \cdot g \,.$$

In the case of non absorbing material:

$$C_{pr} = C_{sca}(1 - g) \,.$$

The asymmetry parameter for spheres has been calculated and analytical or empirical expressions have been derived in the framework of different approximations, e.g. geometrical optics and RGD approximations. Empirical expressions for large randomly oriented non-spherical particles were also proposed (see Kokhanovsky, 2001). Rigorous calculations were achieved by different authors (see, for instance, Xu (1998b)).

Up to now, calculations of radiation pressure cross-section for aggregates have been mainly motivated by the calculation of forces acting on interstellar dust illuminated by stars (Kimura and Mann, 1998; Kimura et al., 2002; Iati et al., 2004). Radiation pressure plays a key role in the dynamical behavior of submicrometer-size grains in the stellar radiation and gravitational fields. Kimura and Mann (1998) studied aggregates composed of 256 primary particles, the radius of which is $0.01\,\mu$m and that are illuminated by visible light and infrared. The considered materials are silicate and amorphous carbon as representatives of weakly and strongly absorbing materials, respectively. Calculations for randomly oriented fractal-like aggregates (with $D_F = 2$ and $D_F = 3$) were performed by means of the DDA method. Authors showed that the asymmetry parameter smoothly increases with increasing

size parameter x (decreasing wavelength) of the primary particle and increases as the fractal dimension decreases if $x < 0.16$ (for $x > 0.16$, $g \simeq 0.7$). The asymmetry parameter for aggregates is higher than for volume-equivalent spheres, irrespective of the constituent material. The authors point out that aggregates with small fractal dimension present a large fluctuation in g for different aggregate orientations. Kimura et al. (2002) extended the previous study to larger aggregates ($N < 2048$). They compare radiation pressure cross-sections calculated from the DDA method, Mie theory applied to volume-equivalent sphere (CS method) and Mie theory combined with the Bruggeman mixing rule. CS is a rough approximation for the two materials and two fractal dimensions. Mie/Bruggeman approximation is a good approximation for compact aggregates, but performs weakly for loose aggregates, especially with non-absorbing primary particles. The authors showed that C_{pr} is less dependent on the porosity of aggregates while the values strongly vary with the material composition. Iati et al. (2004) computed, through the T-matrix method, optical properties of cosmic dust grains. Grains are aggregates consisting of 31 non-identical spheres. Materials are also silicate and amorphous carbon. Primary particle size distribution is assumed to be Gaussian-like. The radius of the volume-equivalent sphere is equal to $0.14\,\mu$m. For both materials, aggregation leads to a sharp increase in the extinction and radiation pressure cross-sections. Subsections 2.5.2 and 2.5.3 are respectively devoted to the main features of C_{pr} for aggregates and approximate methods for estimating C_{pr}.

2.5.2 Main features of radiation pressure cross-section

2.5.2.1 Single sphere

The variation of the asymmetry parameter is presented for spherical particles of various chemical compositions in Fig. 2.19.
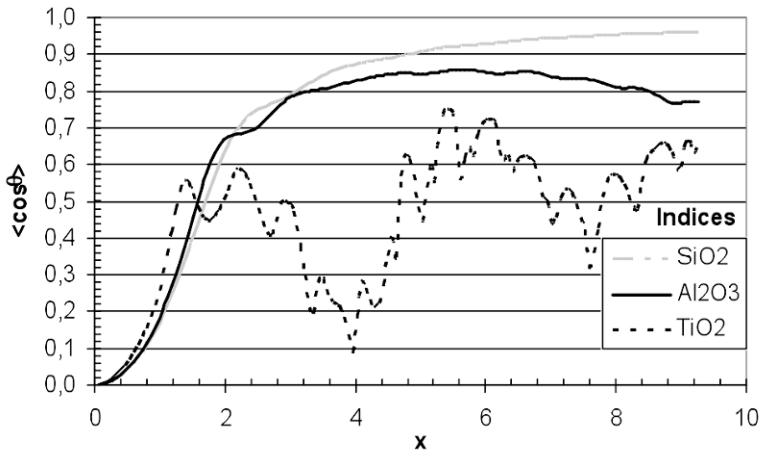

Fig. 2.19. Asymmetry parameter for three materials as function of the size parameter.

The asymmetry parameter is close to zero for very small size parameters, whatever the refractive index. Then, it increases to a plateau close to 1 in the case of SiO_2 and Al_2O_3, i.e. the light is scattered predominantly in the forward direction. A spherical particle of TiO_2 has a mean scattering angle which varies less monotonously according to the size parameter. Indeed, for a size parameter equal to 4, the asymmetry parameter is close to zero, the scattering can be then described as dipole-like, while for a size parameter of about 6 the scattering seems to happen in a privileged direction. Fig. 2.20 represents C_{pr} as a function of the size parameter for a sphere and the three different materials. In the size parameter range [0; 10], the radiation pressure cross-section increases as the optical refractive index increases.
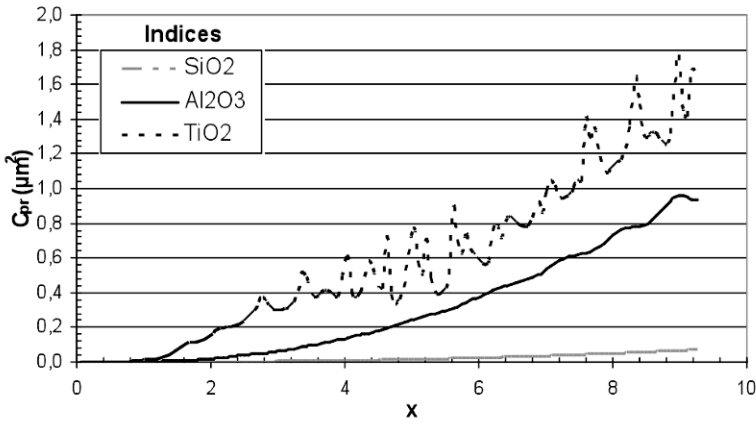

Fig. 2.20. Radiation pressure cross-section for three materials as function of the size parameter.

2.5.2.2 Aggregate of spheres

The variations of C_{pr} for an aggregate have been examined according to: the number of primary particles, their size parameter, the relative optical refractive index and the aggregate shape. Simulations were performed by means of the GMM method (Xu, 1998b).

The simulation results are presented as previously: effect of the number of primary particles within the aggregate and effect of the aggregate shape on the function $P_{Xu}(x)$. P_{Xu} is the ratio between C_{pr} value of an aggregate $(C_{pr,Xu,N})$ and one of its N primary particles considered as independent $NC_{pr,Mie,1}$:

$$P_{Xu} = \frac{C_{pr,Xu,N}}{NC_{pr,Mie,1}} \, .$$

2.5.2.2.1 Effect of the number of primary particles on the radiation pressure cross-section

Fig. 2.21 represents P_{Xu} as a function of the size parameter for a chain-aggregate of SiO_2 primary particles. The variation of C_{pr} with primary particle size parameter is similar to that one corresponding to the scattering cross-section. Two size parameter ranges can be defined. In the x-range $[0; 2]$, constructive interferences and multiple scattering (or interaction between primary particles) are important. In the x-range $[2; 10]$, the radiation pressure cross-section is close to the C_{pr} of a set of spheres without interaction. However, multiple scattering still occurs at some extend.
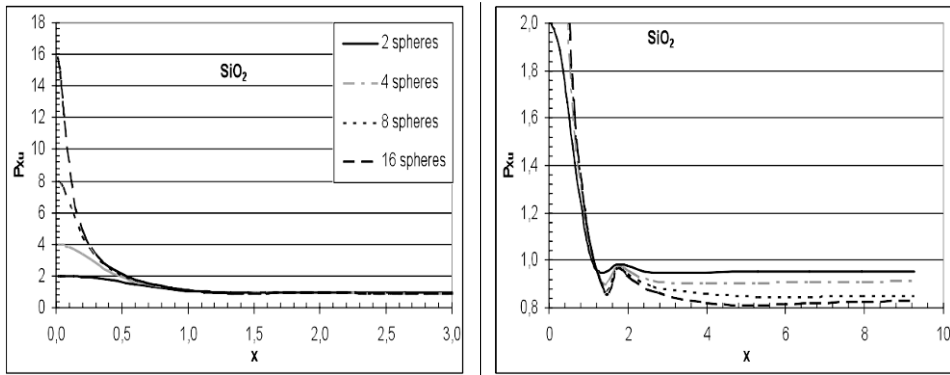

Fig. 2.21. P_{Xu} as a function of the size parameter for the linear configuration with N primary particles (2, 4, 8, 16) and for SiO_2: (a) for the range $x \in [0,3]$ and (b) $x \in [0,10]$.

However, the radiation pressure cross-section of an aggregate made up of primary particles whose size parameter is higher than 1.5 seems to be proportional (by a factor $p(N,x)N$) to the primary particle radiation pressure cross-section. $p(N,x)N$ is a weak function of x for SiO_2 (more dependent on x for TiO_2). As expected, $P_{Xu}(x)$ is similar to $K_{Xu}(x)$ in the x-range $[0; 1]$ because the asymmetry factor of the primary particle is smaller than 0.25. But, $P_{Xu}(x)$ must not be related to $K_{Xu}(x)$ in the x-range $[1; 10]$.

2.5.2.2.2 Effect of the aggregate morphology on radiation pressure cross-section

Fig. 2.22 represents P_{Xu} for different configurations of aggregates consisting of four primary particles arranged according to Fig. 2.9. Similar variations are obtained. The deviation between the two extreme configurations is about 10.7%, which is a smaller value than that obtained with C_{sca}. But C_{pr} is a little more sensitive to configurations which are close each other, since the average deviation between the p1 and p2 configurations is about 1.3% compared with 0.8% for C_{sca}.
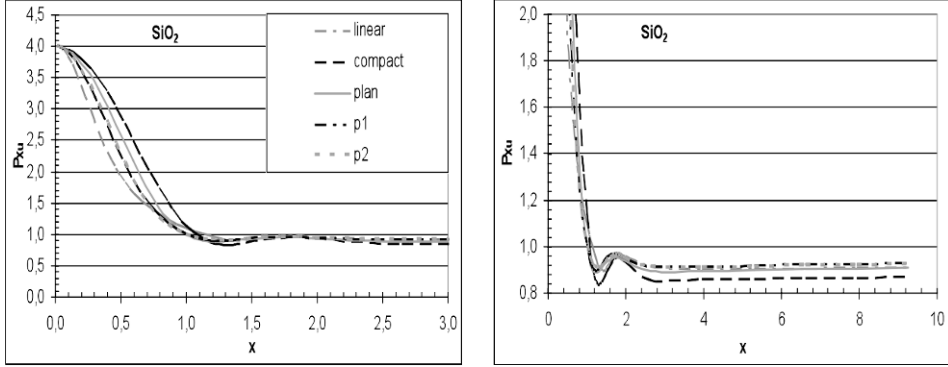
Fig. 2.22. P_{Xu} as a function of the size parameter for different configurations of 4-aggregates (linear, compact, plane, p1, p2) for SiO_2.

2.5.3 Approximate methods for aggregates

2.5.3.1 The ERI method

In the same way that we showed the effectiveness of the ERI approximate method, for calculation of C_{sca}, we evaluated (Jacquier and Gruy, 2007b) its performances for the calculation of C_{pr}. The ratio of the radiation pressure cross-sections obtained on the one hand with the exact (GMM) method and on the other hand with the ERI method is denoted L_m:
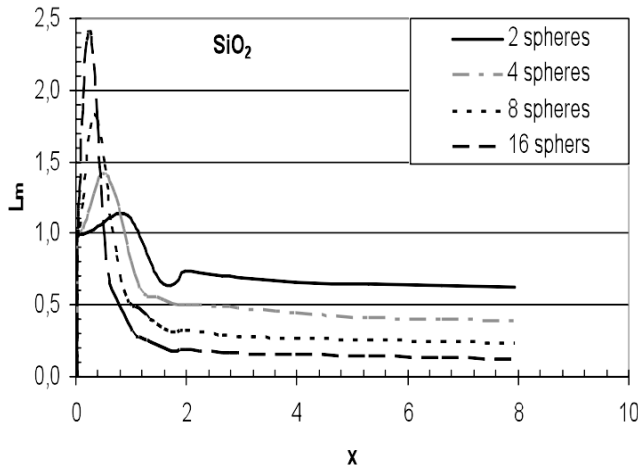
$$L_m = \frac{C_{pr,ERI,N}}{C_{pr,Xu,N}} \ .$$

Fig. 2.23. L_m function with $x \in [0; 10]$ for linear aggregate (SiO_2).

The deviation of L_m from 1 (Fig. 2.23) leads to the search for a corrective factor in order to reduce it. Jacquier and Gruy (2007b) proposed a corrective factor as a multi-parameter function $G(x, N, d_1/a)$ for the radiation pressure cross-section $C_{pr,ERI,N}$. Thus, the corrected radiation pressure cross-section obeys the expression:

$$C_{pr,ERI,N}^{corr} = C_{pr,ERI,N}/G(x, N, d_1/a). \qquad (2.24)$$

Later on, this method is called ERI/G.

2.5.3.2 Other methods

We noticed in subsection 2.5.2.2 that P_{Xu} of any configuration of soft particles does not vary with x for x higher than 1.5. The value of $P_{Xu(x>1.5)}$ depends on the aggregate morphology that can be characterized through N and d_1/a. However, $P_{Xu(x>1.5)}$ may be a weak function of x for hard material (Fig. 2.24). We can observe that variations of $P_{Xu(x>1.5)}$ are similar to those for a two-sphere aggregate.
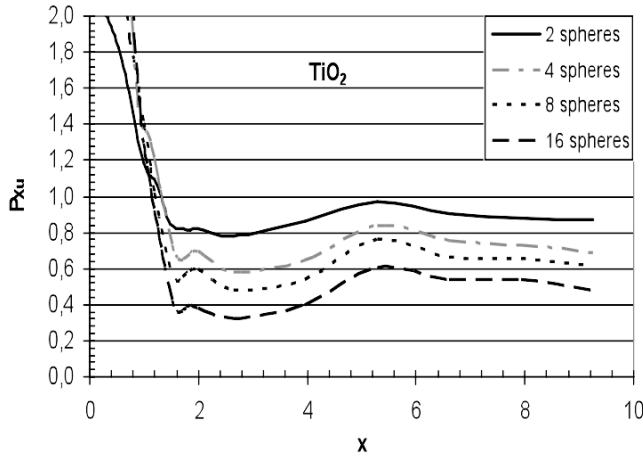
Fig. 2.24. P_{Xu} as a function of the size parameter for the compact configuration with N primary particles (2, 4, 8, 16) and for TiO_2: $x \in [0, 10]$.

These comments suggest the two approximate methods:

- method Pp1: $C_{pr,Xu,N}$ proportional to C_{pr} of a primary particle: $C_{pr,Mie,1}$
- method Pp2: $C_{pr,Xu,N}$ proportional to C_{pr} of a doublet: $C_{pr\,Xu,2}$

The proportionality factors, denoted respectively p_1 and p_2, can be expressed as a function of a single parameter: $\beta = N/\sqrt{d_1/a}$. Corresponding expressions can be found in (Jacquier and Gruy, 2007b). Table 2.3 presents the performances of ERI/G, Pp1 and Pp2. It appears that the ERI/G method is not as efficient as Pp1 and Pp2 but ERI/G presents the biggest advantage to be used over all the size range.

Table 2.3. Approximate method performance for the calculation of C_{pr} for different materials with $x \in [1.5; 10]$. m and σ are respectively the mean value and the standard deviation for the corresponding dataset

method	Linear configuration						Compact configuration					
material	SiO_2		Al_2O_3		TiO_2		SiO_2		Al_2O_3		TiO_2	
	m	σ	m	σ	m	σ	m	σ	m	σ	m	σ
Pp1	1.01	0.05	1.05	0.11	1.06	0.17	1.01	0.04	1.00	0.11	1.08	0.17
Pp2	0.98	0.04	0.96	0.08	0.94	0.12	0.97	0.04	0.93	0.10	0.93	0.11
ERI/G	0.93	0.17	0.90	0.15	1.07	0.23	0.92	0.13	0.90	0.11	1.06	0.30

2.5.4 Conclusion

We have presented different ways to calculate approximately the radiation pressure cross-section of aggregates. The corresponding expressions can be used to study dense suspensions. For instance, Tontrup et al. (2000) performed an experimental work about the aggregation of TiO_2 micro-particles in water by using a backscattering sensor. They deduced the change of the transport mean free path with time. SEM observations showed that the aggregates contain few primary particles. Approximations could be used to determine some characteristics of the aggregates.

2.6 Scattering properties versus geometrical parameters of aggregates

The main question that appears when studying the formation of particles or aggregates is: which is the relevant morphological parameter related to the measurement? The answer mainly depends on the particle size and is partially included in theories and modeling leading to scattering cross-section calculations.

So, when we consider the Mie theory for homogeneous spheres, the solving method and the results are dependent only on the relative refractive index and the boundary conditions for the Helmholtz equation. From a geometrical point of view, the mathematical function describing the particle surface is the relevant parameter. The case of non-spherical convex bodies is similar. As the physics is always based on the Maxwell and Helmholtz equations, the corresponding solution for a natural incident light depends only on the body surface that is characterized by the equation $f(x, y, z) = 0$.

If we are interested in the orientation average of the scattering cross-section, a function describing the body and being invariant to rotation will be preferred. So, the pair distance distribution density (PDDD) could be an interesting approach to describing the shape. It is a well-known function in physics and can be defined for liquids as:

$$dN = g(r)4\pi r^2 \, dr \,.$$

dN represents the number of molecules distant from a given (tagged) molecule with the distance in the range $[r, r + dr]$. In the case of liquid, the distribution is nearly

isotropic. This function clearly appears in RGD approximation for convex bodies (distribution density is connected to $|f|^2$) and BPK approximation for multi-sphere aggregate (in Eqs (2.14a) and (2.14b)).

In the first case (RGD), we consider any pair of volume elements in the scattering body. The pair distance distribution density is a continuous function of the distance between volume elements. In our context, we chose the notation $D_p(r)$. Then, the orientation-averaged scattering cross-section can be written as (Gruy, 2009):

$$C_{RGD,1} = \frac{2}{3\pi} k^4 V^2 (m-1)^2 \int_{R_{min}}^{R_{max}} F(kr) D_p(r) \, dr \qquad (2.25)$$

with

$$F(x) = 3\left[\cos(2x)(-1+5x^{-2}-3x^{-4}) + \sin(2x)(2x^{-1}-6x^{-3}) + 1 + x^{-2} + 3x^{-4}\right]/(4x^2) \, .$$

The distribution density function is normalized:

$$\int_{R_{min}}^{R_{max}} D_p(r) \, dr = 1 \qquad (2.26)$$

Fig. 2.25 presents the function $D_p(r)$ for a sphere and various spheroids. The pair distribution function for a sphere with radius a obeys the expression:

$$aD_p(r) = D_{p,u}(u) = \frac{3}{16} u^2 (u^3 - 12u + 16) \qquad (2.27)$$

with $u = r/a$ and $0 < u < 2$.

In the second case (BPK), equations contain the inter-particle distance d_{ij}. This function is not continuous; as far as a cluster of point scatterers is concerned:

$$D_p(r) = \frac{1}{N(N-1)} \sum_{i,j} \delta(r - d_{ij}) \, . \qquad (2.28)$$

δ is the Dirac function.

A particular case is the fractal-like aggregate, the PDDD of which obeys the equation (continuous form):

$$D_p(r) \propto r^{D_F - 3} \, . \qquad (2.29)$$

According to subsection 2.4.3.2, the BPK approximation gives good results when the size parameter of the primary particle is smaller than 2. Thus, the PDDD is the relevant morphological parameter.

It has been shown by Gruy (2009) that this function associated with BP approximation (Berry and Percival, 1986) for aggregates of Rayleigh scatterers allows for an estimation of the scattering cross-section of convex bodies. This method is proved efficient for spheres and spheroids as the scattering efficiency is smaller than 1 and as the material is optically either soft or hard.

The non-corrected ERI method is based only on the average projected area $\langle S_p \rangle_0$ of the body. However, it is not suitable for elongated aggregates with small size parameter. $\langle S_p \rangle_0$ can be expressed as a function of the number of primary particles and of the mean inter-particle distance (Jacquier and Gruy, 2008a,b):
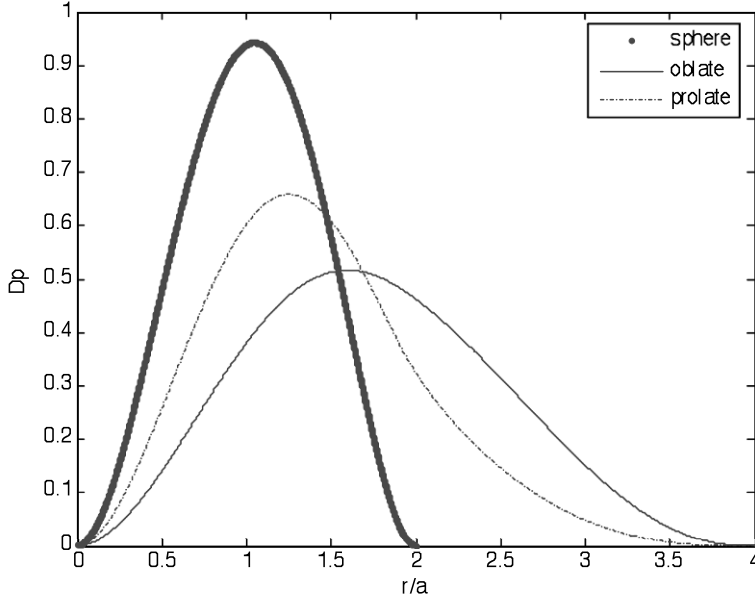
Fig. 2.25. Pair distance distribution density for sphere, oblate spheroid (axis ratio equal to 2) and prolate spheroid (axis ratio equal to 2). a is the smallest semi-axis length.

$$\langle S_p \rangle_0 = \pi R_p^2 \,, \tag{2.30}$$

with $R_p = a(d_1/2a)^{1/5} N^{1/3} d_E^{1/8}$ and $N < 100$; d_E is the space dimension; d_1 is the relevant morphological parameter. It is directly related to the first moment of the distribution $D_p(r)$:

$$
\begin{aligned}
M_1 &= \int_0^\infty D_p(r) r \, dr \\
&= \int_0^\infty \frac{1}{N(N-1)} \sum_{i,j} \delta(r - d_{ij}) r \, dr \\
&= \frac{1}{N(N-1)} \sum_{i,j} d_{ij} = d_1 \,.
\end{aligned}
\tag{2.31}
$$

It would be possible to choose other moments of the distribution for describing geometrical and optical properties of aggregates. For instance, the second-order moment is directly related to the gyration radius, that is a well-known parameter used to define a fractal-like aggregate. However, there was no noticeable change and thus no improvement was found when choosing another mean distance definition for the aggregate. Thus, we chose the lowest-order distribution moment. The corrected ERI method also uses the d_1 distance parameter.

For large size parameter ($x > 2$), the AD approximation becomes efficient. In this case, the relevant line is the chord. Expression of the average scattering cross-section can be rewritten by introducing the chord length distribution $D_l(l)$ (Jacquier and Gruy, 2008a,b):

$$\langle C_{AD,N} \rangle = \left\langle 2 \iint\limits_{[S_p]} \left(1 - \cos kl(m-1)\right) dy\, dz \right\rangle$$

$$\simeq 2\langle S_p \rangle \int_0^{l_{max}} \left(1 - \cos kl(m-1)\right) D_l(l)\, dl \qquad (2.32)$$

The chord length distribution (CLD) is defined as follows: $D_l(l)\, dl$ represents the number fraction of the chord length in the range $[l, l+dl]$. Thus, $D_l(l)$ obeys the normalization equation:

$$\int_0^{l_{max}} D_l(l)\, dl = 1\,. \qquad (2.33)$$

l_{max} is the maximum chord length of an aggregate.

Fig. 2.26 presents the $D_l(l)$ function for an aggregate consisting of 16 primary particles. One observes three very distinct peaks or modes, each one characterized by a chord length range:

– $[0; 2a]$ corresponds to primary particles (distribution density $D_{l,1}(l)$)
– $[2a; 4a]$ corresponds to pair of particles in contact (distribution density $D_{l,2}(l)$)
– $[4a; l_{max}]$ corresponds to the aggregate superstructure (distribution density $D_{l,G}(l)$)

$D_l(l)$ contains the contributions of each distribution density. These are weighted by the coefficients ξ_1, ξ_2, ξ_3:
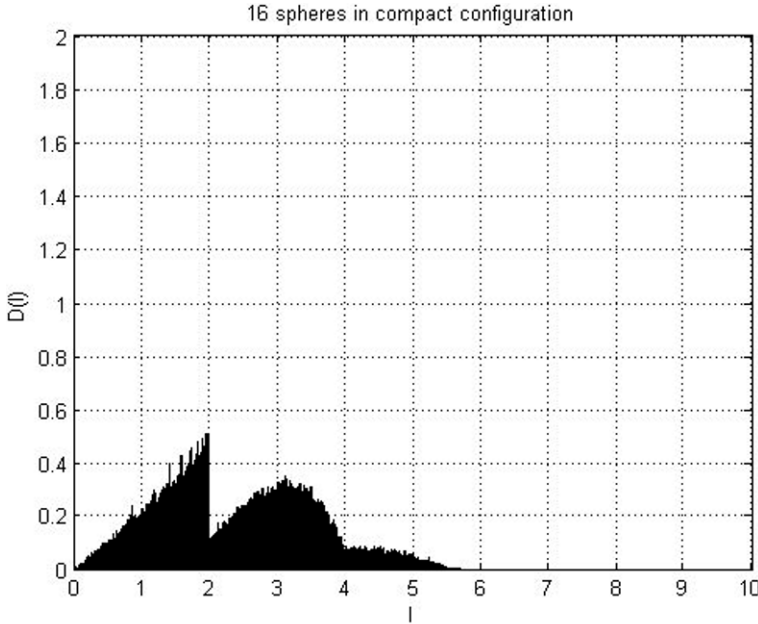

Fig. 2.26. $D_l(l)$ for compact aggregate with 16 primary particles. l is normalized by the radius of the primary particle.

$$D_l(l) = \xi_1 D_{l,1}(l) + \xi_2 \frac{D_{l,2}(l \in [2a; 4a])}{\int_{2a}^{4a} D_{l,2}(l)\, dl} + \xi_G \frac{D_{l,G}(l \in [4a; l_{max}])}{\int_{4a}^{l_{max}} D_{l,G}(l)\, dl} \qquad (2.34a)$$

with

$$\xi_1 + \xi_2 + \xi_G = 1\,. \qquad (2.34b)$$

The distribution densities $D_{l,1}(l)$ and $D_{l,2}(l)$ are given by analytical expressions (Jacquier and Gruy, 2008a,b). $D_{l,G}(l)$ is an empirical function, the same for all the aggregates. Only weighting coefficients depend on the aggregate morphology. Results shown in Fig. 2.26 for a particular aggregate are representative for aggregates with primary particle number up to one hundred. Coefficients ξ_1, ξ_2, ξ_G depend on N, d_1, d_E (Jacquier and Gruy, 2008a,b).

The calculation of the scattering cross-section using Eqs (2.32) to (2.34b)) is much faster than that based on Eq. (2.19).

Certain presented approximations are characterized by a decoupling or separation between optics and geometry. This separation allows for a faster calculation of the optical properties. To our knowledge, the relationship between chord length distribution (as defined by Fig. 2.15) and pair distance distribution is not trivial, particularly for aggregates, and requires complementary works in the field of integral geometry. Moreover, the transition between the different geometrical characteristics, i.e PDD and CLD, as the primary particle size increases is not yet quantitatively understood.

2.7 Conclusion

The analysis of turbidimetric data during the precipitation process is a challenge for researchers working in the field of light scattering by particles. The variety of sizes, shapes and optical contrast requires several approaches for the calculation of their optical properties. Performance criteria are the calculation speed and the accuracy fitted with the measurement accuracy. Accurate calculations performed with sophisticated numerical methods will always be needed and used for the purpose of validation. Difficulties remain for certain particles with a complex morphology. For instance, one observes precipitated zinc sulphide particles in the size range $[0.5\,\mu\text{m}; 5\,\mu\text{m}]$ exhibiting sand rose (i.e., gypsum flower) morphology. The typical multi-scale morphology of many precipitated particles firstly needs tools coming from integral geometry in order to be described with a minimum number of parameters. Knowing this parameter set, optical properties will be calculated with exact theories. The parameter number coming from geometrical analysis can be reduced when the optical properties of the particles are appropriately considered for the formulation of approximate theories to the calculation of scattering properties. An example for such an approach has been presented, but further advances are needed.

Acknowledgment

References

Akkermans, E., P. E. Wolf, R. Maynard, G. Maret, 1988: Theoretical study of the coherent backscattering of light by disordered media, *J. Phys. Fr.*, **49**, 77–98.

Asano, S., 1979: Light scattering properties of spheroidal particles, *Appl. Optics*, **18**(5), 712–723.

Asano, S. and M. Sato, 1980: Light scattering by randomly oriented spheroidal particles. *Appl. Optics*, **19**(6), 962–974.

Asano, S. and G. Yamamoto, 1975: Light scattering by spheroidal particle, *Appl. Optics*, **14**(1), 29–49.

Auger, J.-C., R. G. Barrera, B. Stout, 2003: Scattering efficiency of clusters composed by aggregated spheres, *J. Quant. Spectr. Rad. Transfer*, **79–80**, 521–531.

Auger, J.-C., B. Stout, V. Martinez, 2005: Scattering efficiency of aggregated clusters of spheres: dependence on configuration and composition, *J. Opt. Soc. Am.*, **22**(12), 2700–2708.

Berry, M. V. and I. C. Percival, 1986: Optics of fractal clusters such as smoke, *Opt. Acta*, **33**(5), 577–591.

Bohren, C. F. and D. R. Huffman, 1998: *Absorption and Scattering of Light by Small Particles*, Wiley-VCH, Berlin.

Cameirao, A., R. David, F. Espitalier, F. Gruy, 2008: Effect of precipitation conditions on the morphology of strontium molybdate agglomerates, *J. Cryst. Growth*, **310**, 4152–4162.

Chylek, P. and J. D. Klett, 1991: Absorption and scattering of electromagnetic radiation by prismatic columns: anomalous diffraction approximation, *J. Opt. Soc. Am.*, **8**, 274–281.

Coccioli, R., T. Itoh, G. Pelosi, P. P. Silvester, 1996: Finite elements methods in microwaves: a selected bibliography, *Antennas Propag. Mag.*, **38**, 34–48.

Coudun, C., E. Amblard, J.-C. Guihaumé and J.-F. Hochepied, 2007: Nanostructured particles by controlled precipitation techniques; example of nickel and cobalt hydroxides, *Catal. Today*, **124**, 49–54.

de Wolf, D. A.,1991: Backscatter enhancement: random continuum and particles, *J. Opt. Soc. Am. A*, **8**, 465–471.

Draine, B. T. and P. J. Flatau, 1994: Discrete-dipole approximation for scattering calculations, *J. Opt. Soc. Am.*, **11**(4), 1491–1499.

Elimelech, M., J. Gregory, X. Jia, R. Williams, 1995: *Particle deposition and aggregation, measurement, modelling and simulation*, Butterworth-Heinemann Ltd, Oxford.

Farafonov, V. G., V. B. Il'in, T. Henning, 1999: A new solution of the light scattering problem for axisymmetric particles, *J. Quant. Spectr. Rad. Transfer*, **63**, 205–215.

Fuller, K. A. and G. W. Kattawar, 1988a: Consummate solution to the problem of classical electromagnetic scattering by an ensemble of spheres. I: Linear chains, *Opt. Lett.*, **13**(2), 90–92.

Fuller, K. A. and G. W. Kattawar, 1988b: Cosummate solution to the problem of classical electromagnetic scattering by an ensemble of spheres II: Clusters of arbitrary configuration, *Opt. Lett.*, **13**(12), 1063–1065.

Gruy, F., 2001: Formation of small silica aggregates by turbulent aggregation, *J. Colloid Interf. Sci.*, **237**, 28–39.

Gruy, F., 2009: Light scattering cross-section as a function of pair distribution density, *J. Quant. Spectr. Rad. Transfer*, **110**, 240–246.

Gruy, F. and S. Jacquier, 2008: The chord length distribution of a two-sphere aggregate, *Comp. Mater. Sci.*, **44**, 218–223.

Harrington, R. F., 1968: *Field computation by moment methods*, New York, Macmillan.

Helfenstein, P., J. Ververka, J. Hillier, 1997: The lunar opposition effect, a test of alternative models, *Icarus*, **128**, 2–14.

Hovenier, J.W., K. Lumme, M.I. Mishchenko, N.V. Voshchinnikov, D.W. Mackowski, J. Rahola, 1996: Computations of scattering matrices of four types of non-sphericles using diverse methods, *J. Quant. Spectr. Rad. Transfer*, **55**(6), 695–705.

Iati, M.A., R. Saija, A. Giusto, P. Denti, F. Borghese, C. Cecchi-Pestellini, 2004: Optical properties of interstellar gain aggregates, *J. Quant. Spectr. Rad. Transfer*, **89**, 43–45.

Ishimaru, A., 1978: *Wave Propagation and Scattering in Random Media* (2 vols), Academic Press, New-York.

Ishimaru, A., Y. Kuga, R.L.T. Cheung, K. Shimizu, 1983: Scattering and diffusion of a beam wave in randomly distributed scatterers, *J. Opt. Soc. Am.*, **73**(2), 131–136.

Jacquier, S., 2006: Approximate methods for the optical properties of spherical non-absorbent aggregated particles. PhD thesis, Ecole Nationale Supérieure des Mines de Saint-Etienne, Saint-Etienne.

Jacquier, S. and F. Gruy, 2007a: Approximation of the light scattering cross-section for aggregated spherical non-absorbent particles, *J. Quant. Spectr. Rad. Transfer*, **106**, 133–144.

Jacquier, S. and F. Gruy, 2007b: Approximation for scattering properties of aggregated spherical particles, PARTEC 2007, Nürnberg.

Jacquier, S. and F. Gruy, 2008a: Anomalous Diffraction Approximation for light scattering cross-section: case of ordered clusters of non-absorbent spheres, *J. Quant. Spectr. Rad. Transfer*, **109**, 789–810.

Jacquier, S. and F. Gruy, 2008b: Anomalous Diffraction Approximation for light scattering cross-section: case of random clusters of non-absorbent spheres, *J. Quant. Spectr. Rad. Transfer*, **109**, 2794–2803.

Kahnert, F.M., 2003: Numerical methods in electromagnetic scattering theory, *J. Quant. Spectr. Rad. Transfer*, **79**(80), 775–824.

Khlebtsov, N.G., 1996: Spectroturbidimetry of fractal clusters: test of density correlation function cut-off, *Appl. Optics*, **35**(21), 4261–4270.

Kimura, H. and I. Mann, 1998: Radiation pressure cross-section for fluffy aggregates, *J. Quant. Spectr. Rad. Transfer*, **60**(3), 425–438.

Kimura, H., H. Okamoto, T. Mukai, 2002: Radiation pressure and the Pointing-Robertson effect for fluffy dust particles, *Icarus*, **157**, 349–361.

Kokhanovsky, A.A., 2001: *Light Scattering Media Optics: Problems and Solutions* (2nd edn), Praxis Publishing, Chichester.

Kolokolova, L. and B.A.S. Gustafson, 2001: Scattering by inhomogeneous particles: microwave analog experiments and comparison to effective medium theories, *J. Quant. Spectr. Rad. Transfer*, **70**, 611–625.

Kostoglou M., A.G. Konstandopoulos, S.K. Friedlander, 2006: Bivariate population dynamics simulation of fractal aerosol aggregate coagulation and restructuring, *Aerosol Sci.*, **37**(9), 1102–1115.

Kruyt, H.R., 1952: *Colloid Science*, Elsevier, Amsterdam.

Kuga, Y. and A. Ishimaru, 1984: Retroreflectance from a dense distribution of spherical particles, *J. Opt. Soc. Am.*, **1**(8), 831–835.

Liu, C.-L., 1998: Validity of anomalous diffraction approximation in m-x domain, *Atmos. Res.*, **49**, 81–86.

Liu, Y., W.P. Arnott, J. Hallett, 1998: Anomalous diffraction theory for arbitrarily oriented finite circular cylinders and comparison with exact T-matrix results, *Appl. Optics*, **37**(21), 5019–5030.

Lopatin, V.N. and F.Ya. Sid'Ko, 1988: *Introduction to Optics of Cell Suspensions*, Moscow, Nauka.

Mekki-Berrada, K., F. Gruy, M. Cournil, 2005: *Synthèse d'agglomérats multi-échelles par précipitation homogène (Récents Progrès en Génie des Procédés)* Edition Lavoisier, Paris.

Mishchenko, M. I., D. W. Mackowski, L. D. Travis, 1995: Scattering of light by bispheres with touching and separated components, *Appl. Optics*, **34**(21), 4589–4599.

Mishchenko, M. I., L. D. Travis, and A. A. Lacis, 2002: *Scattering, Absorption, and Emission of Light by Small Particles*, Cambridge University Press, Cambridge.

Mishchenko, M. I., G. Videen, V. A. Babenko, N. G. Khlebtsov, T. Wriedt, 2004: T-matrix theory of electromagnetic scattering by particles and its applications: a comprehensive reference database, *J. Quant. Spectr. Rad. Transfer*, **88**, 357–406.

Mishchenko, M. I., G. Videen, V. A. Babenko, N. G. Khlebtsov, T. Wriedt, 2007: Comprehensive T-matrix reference database: A 2004–06 update, *J. Quant. Spectr. Rad. Transfer*, **106**, 304–324.

Mishchenko, M. I., G. Videen, N. G. Khlebtsov, T. Wriedt, N. T. Zakharova, 2008: Comprehensive T-matrix reference database: A 2006–07 update, *J. Quant. Spectr. Rad. Transfer*, **109**, 1447–1460.

Nichols, M. G., E. L. Hull, T. H. Forster, 1997: Design and testing of a white-light, steady-state diffuse reflectance spectrometer for determination of optical properties of highly scattering systems, *Appl. Optics*, **36**, 93–104.

Quirantes, A., F. Arroyo, et al., 2001: Multiple light scattering by spherical particle systems and its dependence on concentration; a T-matrix study, *J. Colloid Interf. Sci.*, **240**, 78–82.

Randolph, A. D., and M. A. Larson, 1988: *Theory of Particulate Processes*, Academic Press, New York.

Rouleau, F., 1996: Electromagnetic scattering by compact clusters of spheres, *Astron. Astrophys.*, **310**, 686–698.

Streekstra, G. J., A. G. Hoekstra, et al., 1994: Anomalous diffraction by arbitrarily oriented ellipsoids: applications in ektacytometry, *Appl. Optics*, **33**, 7288–7296.

Sugimoto, T., 2000: *Fine Particles: Synthesis, Characterization, and Mechanisms of Growth*, (Surfactant Science Series, Vol. 92), Marcel Dekker, New York.

Sun, W. and Q. Fu, 1999: Anomalous diffraction theory for arbitrarily oriented hexagonal crystals, *J. Quant. Spectr. Rad. Transfer*, **63**, 727–737.

Sun, W. and Q. Fu, 2001: Anomalous diffraction theory for randomly oriented nonspherical particles: a comparison between original and simplified solutions, *J. Quant. Spectr. Rad. Transfer*, **70**, 737–747.

Tandon, P., D. E. Rosner, 1999: Monte Carlo Simulation of Particle Aggregation and Simultaneous Restructuring, *J. Colloid and Interf. Sci.*, **213**, 273–286.

Tontrup, C., F. Gruy and M. Cournil, 2000: Turbulent aggregation of titania in water, *J. Colloid and Interf. Sci.*, **229**, 511–525.

Tsang, L., and A. Ishimaru, 1984: Backscattering enhancement of random discrete scatterers, *J. Opt. Soc. Am.*, **1**, 836–839.

Tsang L., and A. Ishimaru, 1985: Theory of backscattering enhancement of random discrete isotropic scatterers based on the summation of all ladder and cyclical terms, *J. Opt. Soc. Am. A*, **2**, 1331–1338.

Van de Hulst, H. C., 1981: *Light Scattering by Small Particles*, Dover publications Inc., New York.

Videen, G. and P. Chylek, 1998: Anomalous diffraction approximation limits, *Atmos. Res.*, **49**, 77–80.

Voshchinnikov, N. V. and V. G. Farafonov, 1992: Optical properties of spheroidal particles, *Astrophys. Space Sci.*, **204**, 19–86.

Wolf, P. E., G. Maret, E. Akkermans, R. Maynard, 1988: Optical coherent backscattering by random media: an experimental study, *J. Phys. Fr.*, **49**, 63–75.

Wriedt, T., 1998: A review of elastic light scattering theories, *Part. Part. Syst. Charact.*, **15**, 67–74.

Xu, Y.-L., 1995: Electromagnetic scattering by an aggregate of spheres, *Appl. Optics*, **34**(21), 4573–4588.

Xu, Y.-L., 1996: Calculation of the addition coefficients in electromagnetic multisphere-scattering theory, *J. Comput. Phys.*, **127**, 285–298.

Xu, Y.-L., 1997a: Electromagnetic scattering by an aggregate of spheres: far field, *Appl. Optics*, **36**(36), 9496–9508.

Xu, Y.-L., 1997b: Fast evaluation of gaunt coefficients: recursive approach, *J. Comput. Appl. Math.*, **85**, 53–65.

Xu, Y.-L., 1998a: Efficient evaluation of vector translation coefficients in multiparticle light-scattering theories, *J. Comput. Phys.*, **139**, 137–165.

Xu, Y.-L., 1998b: Electromagnetic scattering by an aggregate of spheres: asymmetry parameter, *Phys. Lett. A*, **249**, 30–36

Xu, Y.-L. and B. A. S. Gustafson, 2001: A generalized multiparticle Mie-solution: further experimental verification, *J. Quant. Spectr. Rad. Transfer*, **70**, 395–419.

Yang, P. and K. Liou, 2000: Finite difference time domain method for light scattering by nonspherical and inhomogeneous particles. In *Light Scattering by Nonspherical Particles: Theory, Measurements, and Applications*, eds. M. I. Mishchenko, J. W. Hovenier, and L. D. Travis, Academic Press, San Diego.

Yang, P., Z. Zhang, B. A. Baum, H. L. Huang, Y. X. Hu, 2004: A new look at anomalous diffraction theory (ADT): Algorithm in cumulative projected-area distribution domain and modified ADT, *J. Quant. Spectr. Rad. Transfer*, **89**, 421–442.